

Emma Nika Ciric

# Methane Escape from Lowland Terrestrial Seepages

Links to Deglaciation and Permafrost Dynamics



**UNIVERSIDADE DO ALGARVE**  
FACULDADE DE CIÊNCIAS E TECNOLOGIA

2019

Emma Nika Ciric

# Methane Escape from Lowland Terrestrial Seepages

Links to Deglaciation and Permafrost Dynamics

Master in Marine and Coastal Systems

Universidade do Algarve

Supervisors:

Andrew J. Hodson (UNIS)

Óscar M.F.C. Ferreira (CIMA, UAlg)



**UNIVERSIDADE DO ALGARVE**  
FACULDADE DE CIÊNCIAS E TECNOLOGIA

2019

# Methane Escape from Lowland Terrestrial Seepages

Links to Deglaciation and Permafrost Dynamics

“Declaro ser a autora deste trabalho, que é original e inédito. Autores e literatura consultados estão devidamente citados no texto e constam da listagem de referências incluída.”

“I declare I am the author of this work, which is original and unpublished. Authors and literature consulted have been cited in the text and are included in the list of references.”



---

Emma Nika Ciric

“A Universidade do Algarve reserva para si o direito, em conformidade com o disposto no Código do Direito de Autor e dos Direitos Conexos, de arquivar, reproduzir e publicar a obra, independentemente do meio utilizado, bem como de a divulgar através de repositórios científicos e de admitir a sua cópia e distribuição para fins meramente educacionais ou de investigação e não comerciais, conquanto seja dado o devido crédito ao autor e editor respetivos.”

“The University of the Algarve reserves the right, in accordance with the provisions of the Code of the Copyright Law and related rights, to file, reproduce and publish this work, regardless of the used mean, as well as to disseminate it through scientific repositories and to allow its copy and distribution for purely educational or research purposes and noncommercial purposes, although due credit will be given to the respective author and publisher.”

## **Acknowledgements**

Completing this degree would not have been possible without the support of my family and my friends. My mother Valentina, my brother Boris, and my dog Schneider gave me so much strength these past two years. I would also like to thank my wonderful friends in Canada, Portugal, and Svalbard that encouraged me and lifted me up even when I doubted myself. Thank you to Naomi and Craig for your meticulous editing and for letting me ramble about pingos for hours on end.

I would also like to thank Dr. Óscar Ferreira for accepting me into MACS and being a kind and reliable advisor during my time in Portugal and in Svalbard. He was always ready to help me when I needed it, even when it involved signing (and faxing!) a thousand documents from Ontario. My life would be very different today had I not been accepted to the University of the Algarve.

I want to thank Dr. Andy Hodson for seeing something in me and bringing me to Svalbard. Not only was he a caring and supportive supervisor, but he took me snowmobiling hundreds of kilometers across glaciers and sea ice and had me clambering up steep cliffs with a rifle on my back. The field work I got to do in Svalbard was truly special.

I was lucky to have two supervisors who were encouraging and supportive of me even through health challenges. I would also like to thank my incredible friends, in no particular order- Laura, Dannie, Curtis, Carly, Dan, Rosalie, Chris, and Gustavo for giving me their ear whenever I needed to vent about my thesis.

I have become a very different person in the past two years. I am very lucky to have been supported by such wonderful people during my Master's degree.

Muita obrigada! Tusen takk!

## Abstract

In the Norwegian archipelago of Svalbard, 90%-100% of exposed land is underlain by continuous permafrost. Permafrost is estimated to store over 1600 gigatons of carbon worldwide. Pingos, features that only exist in permafrost, ventilate methane in much the same manner as pockmarks can ventilate methane clathrates on the ocean floor. In winter 2019, pingos identified on satellite imagery were studied in the field via water samples. This was done to better understand these uncommon periglacial features and of the methane they release.

A database was created using elevation datasets, GIS analysis, winter satellite photography, and geological data to identify pingos in Svalbard as well as the factors that influence their formation and behaviour. The spatial distribution of pingos and fault lines suggests a relationship between fault zones and the formation of pingos, possibly due to the discontinuity caused by the faults allowing for easier flow of groundwater.

In addition, carbon dioxide and methane had a correlation which is probably associated to the microbial processes leading to the formation of methane. Deuterium was another important compound, likely due to the marine sediments within the Holocene marine limit. A predictive model was then established to show the relationship of carbon dioxide and deuterium with methane. This model estimates the amount of methane ventilated based on other compounds measured in pingos. By combining these scientific approaches, this data provides a step forward in understanding methane reservoirs within permafrost environments, particularly relevant in an unstable and changing climate.

**Keywords:** Svalbard; methane ventilation; open system pingos; continuous permafrost; GIS; Arctic hydrology

## Resumo

No arquipélago norueguês de Svalbard, 90% a 100% da terra exposta assenta em permafrost. Estima-se que o permafrost armazene mais de 1600 gigatoneladas de carbono, em todo o mundo. Pingos são morfologias que só existem no permafrost e que ventitam metano da mesma maneira que as pockmarks podem ventilar clatratos de metano no fundo do oceano. No inverno de 2019, os pingos identificados por imagens de satélite foram estudados no campo, através de amostras de água. Tal foi feito para melhor se entender as características destas incomuns estruturas periglaciais e o metano que elas libertam.

Foi criada uma base de dados que congrega um conjunto de dados de elevação, análise de SIG, fotografia de satélite de inverno e dados geológicos que permitem identificar os pingos. A distribuição espacial dos pingos em relação às linhas de falhas parece indicar uma relação entre as zonas de falha e a formação de pingos, possivelmente devido às descontinuidades causadas pelas falhas, permitindo um fluxo mais fácil das águas subterrâneas.

Além disso, verificou-se que o dióxido de carbono e o metano estão correlacionados, o que é provavelmente devido aos processos microbianos que levam à formação de metano. O deutério foi outro composto importante, provavelmente devido aos sedimentos marinhos dentro do limite marinho do Holocénico. Um modelo preditivo foi então estabelecido para mostrar a relação do metano com dióxido de carbono e deutério. Este modelo estima a quantidade de metano ventilada com base em outros compostos medidos em pingos. Ao combinar várias abordagens científicas, estes dados são um passo em frente na compreensão dos reservatórios de metano em ambientes de permafrost, particularmente relevantes numa situação climática instável e em mudança.

# Table of Contents

Sumário .....	x
1. Introduction.....	1
2. Study Area .....	4
2.1 Geography.....	4
2.2 Geology.....	5
2.3 Historical Glaciation and Climate.....	7
2.4 Current Climate Trends.....	9
3. Literature Review.....	12
3.1 Glaciers .....	12
3.2 Pingos.....	13
3.3 Permafrost .....	14
3.4 Arctic Hydrology .....	16
3.5 Methane Ventilation.....	17
3.6 Microbes as a Source of Methane .....	18
4. Materials and Methods.....	20
4.1 Cartography.....	20
4.2 Sampling in the Field .....	21
4.3 Statistical Analysis .....	23
5. Results.....	24
5.1 Spatial Distribution of Pingos .....	24
5.2 Methane in Nordenskiöld Land.....	27
5.3 Elements of Pingo Formation .....	30
5.4 Relationship Between Methane and Other Compounds .....	35
6. Discussion .....	39
6.1 Physical Geography of Pingos on Svalbard.....	39
6.2 Compounds Associated with Methane.....	42
6.3 Limitations .....	44
7. Conclusion .....	45
8. References.....	47
9. Appendix.....	55

## Index of Figures and Tables

Figure 1.1. Lagoon Pingo in Spitsbergen, Svalbard with two snowmobiles for scale.....	2
Figure 2.1. The Arctic Ocean and its marginal seas.....	5
Figure 2.2. Svalbard’s stratigraphic regions.....	6
Figure 2.3. Location map representing the Svalbard archipelago.....	7
Figure 2.4. The Svalbard-Barents ice sheet during the LGM.....	8
Figure 2.5. Historical average temperatures in Longyearbyen and hours of sunlight.....	10
Figure 2.6. Global temperature anomalies from 2000-2009.....	11
Figure 3.1. Schematic of a pingo in Kunlun Mountain, China.....	14
Figure 3.2. Permafrost distribution in the circumpolar north.....	16
Figure 3.3. An example of an icing in Adventdalen, Spitsbergen, Svalbard.....	17
Figure 4.1. Water from a groundwater icing being passed through membrane detectors.....	22
Figure 4.2. A Pro Oceanus laser detector measuring methane in July 2019.....	22
Figure 5.1. Location of all identified (98) pingos (purple circles) at Svalbard.....	24
Figure 5.2. The locations of pingo-associated icings on Svalbard.....	25
Figure 5.3. Colour-coded groundwater icings on Nordenskiöld Land.....	26
Figure 5.4. Pingo elevations throughout the archipelago of Svalbard.....	27
Figure 5.5. Locations of the four pingos sampled between 2015 and 2017 in Adventdalen.....	27
Figure 5.6. The locations of winter sites in Nordenskiöld Land visited in 2019.....	28
Figure 5.7. Methane at different sites visited in Nordenskiöld Land in winter of 2019.....	29
Figure 5.8. High methane release is generally associated with low oxygen release.....	30
Figure 5.9. Known fault lines on Svalbard relative to the position of pingos.....	31
Figure 5.10. Distance of pingos on Spitsbergen to the nearest fault in kilometers.....	32
Figure 5.11. Pingos closely associated with major fault lines on Andrée Land.....	32
Figure 5.12. Pingos closely associated with major fault lines on Wedel Jarlsberg Land.....	33
Figure 5.13. Pingos closely associated with major fault lines on Nordenskiöld Land.....	34
Figure 5.14. Example of three pingo groups in valleys on Svalbard.....	35
Figure 5.15. Index of pingos relative to their position in the valleys.....	35
Figure 5.16. Linear regression of methane with deuterium.....	37
Figure 5.17. Linear regression of methane with carbon dioxide .....	38

Table 5.1. Component analysis from four pingos in Adventdalen, Spitsbergen, Svalbard.....	36
Table 5.2. Regression statistics for methane with carbon dioxide and deuterium.....	37
Appendix Table 0.1. The locations and parameters measured at icings in Nordenskiöld Land.....	55
Appendix Table 0.2. Data taken from Adventdalen pingos years 2015 to 2017.....	57
Appendix Table 0.3. A list of the 98 pingos found on Spitsbergen and Edgeøya.....	60

## Sumário

O permafrost é um estado térmico descrito como solo que permanece abaixo de 0 ° C por dois ou mais anos. O permafrost está subjacente a 25% da área total da terra, mas não foi ainda adequadamente estudado porque ocorre principalmente em regiões polares e alpinas isoladas. No arquipélago norueguês de Svalbard, 90% a 100% da terra exposta assenta em permafrost, sendo que 60% da área total de Svalbard se encontra coberta por glaciares. Estima-se que o permafrost armazene mais de 1600 gigatoneladas de carbono em todo o mundo. Quando o permafrost derrete, o carbono é libertado na forma de dióxido de carbono ou de metano. O metano é liberado em quantidades menores que o dióxido de carbono, mas os seus efeitos no aquecimento da atmosfera são 28 vezes mais fortes que os do dióxido de carbono. Embora exista um grau considerável de investigação sobre hidratos de metano emanados no oceano, pouco se sabe sobre os reservatórios de metano no permafrost, em terra.

Pingos são morfologias que só ocorrem no permafrost, no Ártico e no subártico, e que ventilam metano da mesma maneira que as pockmarks podem ventilar clatratos de metano no fundo do oceano. Pingos são morfologias que se assemelham a colinas e que ocorrem isoladamente ou em pequenos grupos, em terrenos baixos, como vales ou planícies costeiras. Em Svalbard, a elevação isostática foi superior à subida do nível médio do mar. Isso permitiu que antigas pockmarks marinhas se tornassem pingos através da injeção de água subterrânea. As injeções de água subterrânea que formam coberturas de gelo (icings) são geralmente ricas em metano proveniente de reservatórios em profundidade, de sub-permafrost. A água é originária dos glaciares de Svalbard e também podem formar coberturas de gelo nas moreias terminais dos glaciares. As coberturas de gelo associadas a pingos apresentaram as maiores taxas de emissão de metano e, portanto, foram o foco deste trabalho. Os pingos e hidrologia associada foram pouco estudados, particularmente em regiões de Svalbard que não são facilmente acessíveis. No inverno de 2019, os pingos foram estudados através de imagens de satélite e amostragem de água, no campo. Tal foi efetuado para melhor entender as características destas incomuns estruturas periglaciais e o metano que elas libertam. Dados suplementares recolhidos nos anos de 2015-2017 foram utilizados para estimar a emissão de metano e sua relação com a libertação de outros compostos.

Foram identificados 98 pingos em Svalbard, encontrados apenas nas ilhas de Spitsbergen e Edgeøya. Spitsbergen é a única ilha com coberturas de gelo em água subterrânea associadas a pingos. A maioria das coberturas de gelo ocorre na península de Nordenskiöld Land, no centro de Spitsbergen, e, assim, esses pingos foram o foco deste trabalho. A distribuição espacial dos pingos e de linhas de falha parece indicar uma relação entre as zonas de falha e a formação de pingos, possivelmente devido à descontinuidade nas rochas, facilitando o fluxo das águas subterrâneas. Apenas vinte e cinco pingos na ilha de Spitsbergen estavam localizados a mais de dez quilômetros da falha mais próxima e 33,7% dos pingos em Spitsbergen estavam a um quilômetro ou menos da falha mais próxima. Muitos desses pingos aparecem alinhados de forma paralela às linhas de falha que ocorrem nos vales e ao lado delas.

Um modelo preditivo foi estabelecido para estimar a quantidade de metano ventilada, tendo por base outros compostos medidos em pingos que estão dentro do Holocénico. Foi ainda criado um banco de dados usando conjuntos de dados de elevação, análise em SIG, fotografia de satélite de inverno e dados geológicos. O objetivo foi identificar os pingos em Svalbard, bem como os fatores que influenciam a sua formação e o seu comportamento. As coberturas de gelo associadas a pingos eram mais abundantes na península de Nordenskiöld Land, no centro de Spitsbergen. Em Svalbard, as maiores quantidades de metano libertado, identificadas até agora, estão no vale de Adventdalen, perto da povoação de Longyearbyen. O metano libertado nas coberturas de gelo associadas a pingos atingiu 59% neste vale.

Além disso, verificou-se que o dióxido de carbono e o metano estão correlacionados, provavelmente devido aos processos microbianos que levam à formação de metano. O deutério também está intimamente relacionado com o metano, provavelmente em associação com os sedimentos marinhos localizados dentro do limite marinho do Holocénico. O metano nos pingos é de origem biogénica devido à decomposição de materiais orgânicos. A ventilação de metano ocorre a taxas muito mais altas no inverno do que no verão. Tal decorre do degelo no verão que dilui a água e das bactérias metanogénicas estarem inativas no inverno, permitindo maior libertação de metano. Num clima em mudança, é importante entender o comportamento e a quantidade de libertação de metano no Ártico. Mais investigação de campo deve ser feita em pingos em Svalbard, particularmente em outras áreas de Spitsbergen que logisticamente não são fáceis de alcançar. O metano é um dos principais gases de estufa, e o aumento da sua libertação

pode ser prejudicial para o Ártico. O IPCC considerou Svalbard como um ambiente climático sensível e em grande risco de aquecimento devido a um feedback positivo e à amplificação polar do efeito climático. Ao combinar as abordagens científicas descritas, espera-se que estes dados sejam um passo importante na compreensão dos reservatórios de metano em ambientes de permafrost, particularmente relevantes em situações de instabilidade e mudança climática.

# 1. Introduction

There have been many studies on submarine methane hydrate ventilation, but little research has been published on this phenomenon occurring on land (Stotler et al, 2010). Understanding the dissociation of methane hydrates is vital for recognizing the impact of these features on both the ocean and the atmosphere. The Arctic has stored a vast quantity of methane in permafrost because low annual temperatures prevent the decay of organic matter. Permafrost alone is estimated to contain 720 gigatons of organic carbon globally (Zimov et al, 2006). Svalbard, an archipelago that is part of the Norwegian Arctic, is 60% glaciated with its remaining land area underlain by continuous permafrost. Since the end of the Little Ice Age in the early 20<sup>th</sup> century and with global climate change in recent decades, Svalbard has seen an increase in annual temperatures (Norwegian Meteorological Institute, 2011). This increase in temperature is most pronounced in winter. With a low mean annual precipitation, cold winter temperatures are necessary for the preservation of sea ice, permafrost and glaciers. In the summer of 2012, a record minimum of sea ice was reached in Svalbard (Nordli et al, 2014; Metfies et al, 2016). The loss of sea ice, thinning of glaciers, and thaw of permafrost would have local as well as global consequences.

Svalbard, Norway is an excellent place to study the behaviour of methane because it is a unique environment even when compared to other regions in the High Arctic. It is surrounded by shallow seas that contain methane hydrates. Methane is kept from disassociating due to low temperatures and high pressure. Because of isostatic rebound that has occurred since the end of the Last Glacial Maximum, uplift of Svalbard has outpaced rising sea levels (Ingólfsson, 2011). Isostatic uplift better enables methane to ventilate to the atmosphere (Wallmann et al, 2018). In coastal waters surrounding Svalbard, the dissociation of methane clathrates could occur more frequently if bottom water temperatures are increased. On land, methane ventilation can be facilitated by unique periglacial structures known as pingos (figure 1.1). These are conical, ice-cored hills that can only exist in continuous permafrost. The remnants of pingos can be indicators of past periglacial environments. Most studies have been completed on the island of Spitsbergen, the largest island in Svalbard. Because it is the only island that has permanent human settlements, it is the most accessible region for research.



Figure 1.1. Lagoon Pingo in Spitsbergen, Svalbard with two snowmobiles for scale. Photograph taken by Craig Hammock in March 2019.

Recent studies suggest that pingos on coastlines form because of the occurrence of pockmarks occurring in shallow bays, fjords, estuaries, and other bodies of water (Hodson et al, 2019). Open-system pingos in parts of Svalbard that were once below the marine limit are thought to originate from former pockmarks. Pockmarks are particularly well-preserved in glacio-marine sediments (Portnov et al, 2016). Pingos presently exist in many parts of coastal Spitsbergen that were recovered from the sea due to isostatic uplift and the reduction of glacial ice. These features release a small amount of methane each year. Although a significant amount of this methane is consumed by methanotrophic bacteria in the sediment in summer, these bacteria are inactive in winter and so methane emissions are significantly increased during this season (Hodson et al, in review). Future research should consider how much methane is being added to the atmosphere by these features (Marín-Moreno et al, 2013). Although many papers have been written on the release of methane by pockmarks and pingos in the ocean (e.g. Paull et al, 2007; Forwick et al, 2009; Riedel et al, 2018), relatively little attention has been given to these features on land. In light of warming temperatures and increased global attention on the Arctic, it would be educative to research how methane seepage on land will contribute to the overall volume of carbon in the atmosphere.

The main goal of this research topic was to research pingos on Svalbard and the quantity of methane they ventilate to the atmosphere. To accomplish this, the active emission of methane was examined on Spitsbergen, Svalbard, Norway. Factors such as electroconductivity, PH, and other chemicals were also measured. Using GIS, the concentration and distribution of features that may be associated with methane release were characterized. Pingos were the main focus of

the study as well as associated groundwater icings. The amount of gaseous methane released from these icings in 2019 was quantified and compared to results on four major pingos researched in central Spitsbergen from 2015-2017. Component analyses and multiple regression were two statistical methods used to identify compounds associated with methane. Throughout geologic history, freeze-thaw cycles in permafrost and methane ventilation have occurred as part of natural cycles. However, in a warming climate this natural process is changing and needs to be studied. Understanding these processes in the past and in the present is necessary to comprehend the future behaviour of methane ventilation in a warming climate.

## 2. Study Area

### 2.1 Geography

Svalbard is an archipelago measuring about 63 000 km<sup>2</sup>. It is international territory that is administrated by Norway, located between latitudes 74° to 81° N and from longitudes 10° to 35° E. Located in the Arctic Circle, the closest landmass is Greenland to the west. The islands are located between the Barents Sea to the east, the Greenland Sea to the west, the Norwegian Sea to the south, and the Arctic Ocean to the north (figure 2.1). In most parts of the world, soil, vegetation, and anthropogenic activities have made geological formations indistinct to the naked eye. However, Svalbard acts as a natural archive of the earth's geological history. There are relatively few animals and plants found on the island because of the extreme climate (Rønning, 1996). Winter lasts from October to May and summer from June to September. Often, snow and ice from winter will persist into the month of June. There has been very little human development due to historically limited human habitation. Svalbard has never had an indigenous human population.

Apart from humans and domestic dogs, there are only three terrestrial mammals- Svalbard reindeer (*Rangifer tarandus platyrhynchus*), southern vole (*Microtus levis*), and the Arctic fox (*Vulpes lagopus*). The coasts have a multitude of marine mammals including polar bears, walruses, seals, and many species of migratory whales and dolphins. Svalbard is also the breeding ground of many migratory seabirds such as the Arctic tern and black-legged kittiwake. Because of the polar latitude, the growing season for plants in Svalbard is only a few weeks long. Permafrost beneath the surface of the soil prevents roots from growing very deep. Consequently, plants on Svalbard are rarely higher than 10 cm in height. The biome of Svalbard's largest island, Spitsbergen, is designated as an Arctic tundra, and so many Arctic plants such as *Saxifraga sp.*, *Salix sp.*, *Potentilla sp.*, and *Ranunculus sp.* are found throughout the island (Rønning, 1996).

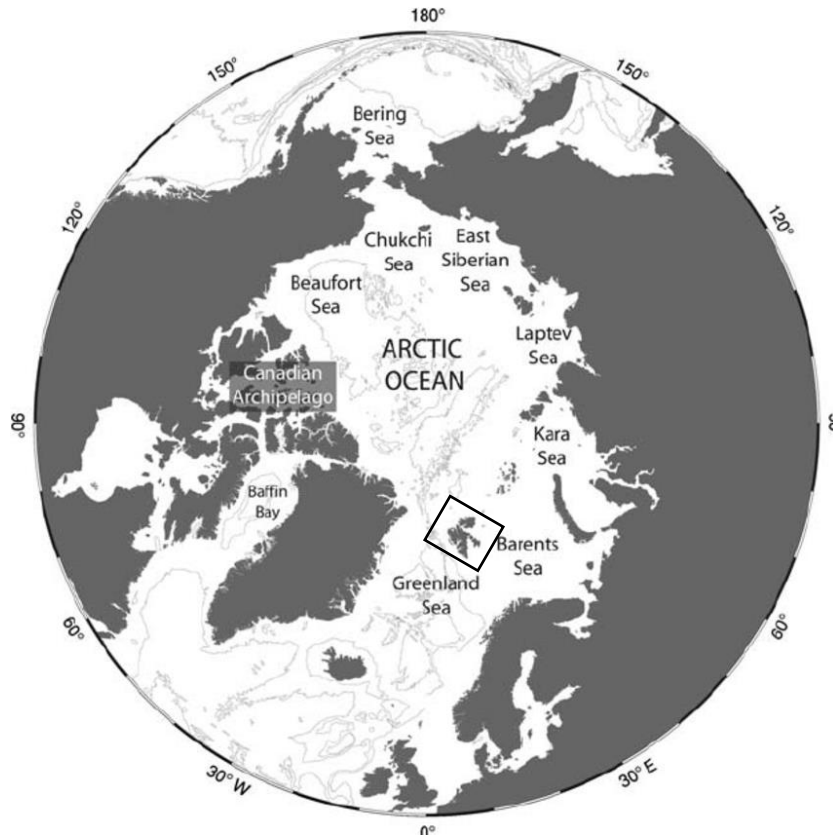


Figure 2.1. The Arctic Ocean and its marginal seas (Piepenburg, 2005). Svalbard is located within the confines of the black box.

## 2.2 Geology

The islands of Svalbard have a basement complex of igneous and metamorphic rocks as well as sedimentary covers deposited from the Devonian to the Permian periods (Hjelle, 1993). Svalbard also has a great deal of unconsolidated deposits from the erosion of glaciers (Norwegian Polar Institute, 2015). Presently, 60% of the islands are covered in glacial ice and polythermal glaciers. The landforms of Svalbard have been affected by multiple glacial periods that have eroded valleys and deposited sediments that influence its environment today (Benn and Evans, 2014). Furthermore, Svalbard is geologically unique because of how well-preserved its stratified sedimentary layers are (figure 2.2). Because the islands were below sea level for much of history, deposition has occurred in nearly perfect stratified columns. Today, this stratification is plainly visible because of the lack of vegetation on the island. The bedrock lies open and exposed, revealing the ancient basement from the Precambrian period all the way to the unconsolidated sediment of the Quaternary period (Hjelle, 1993).

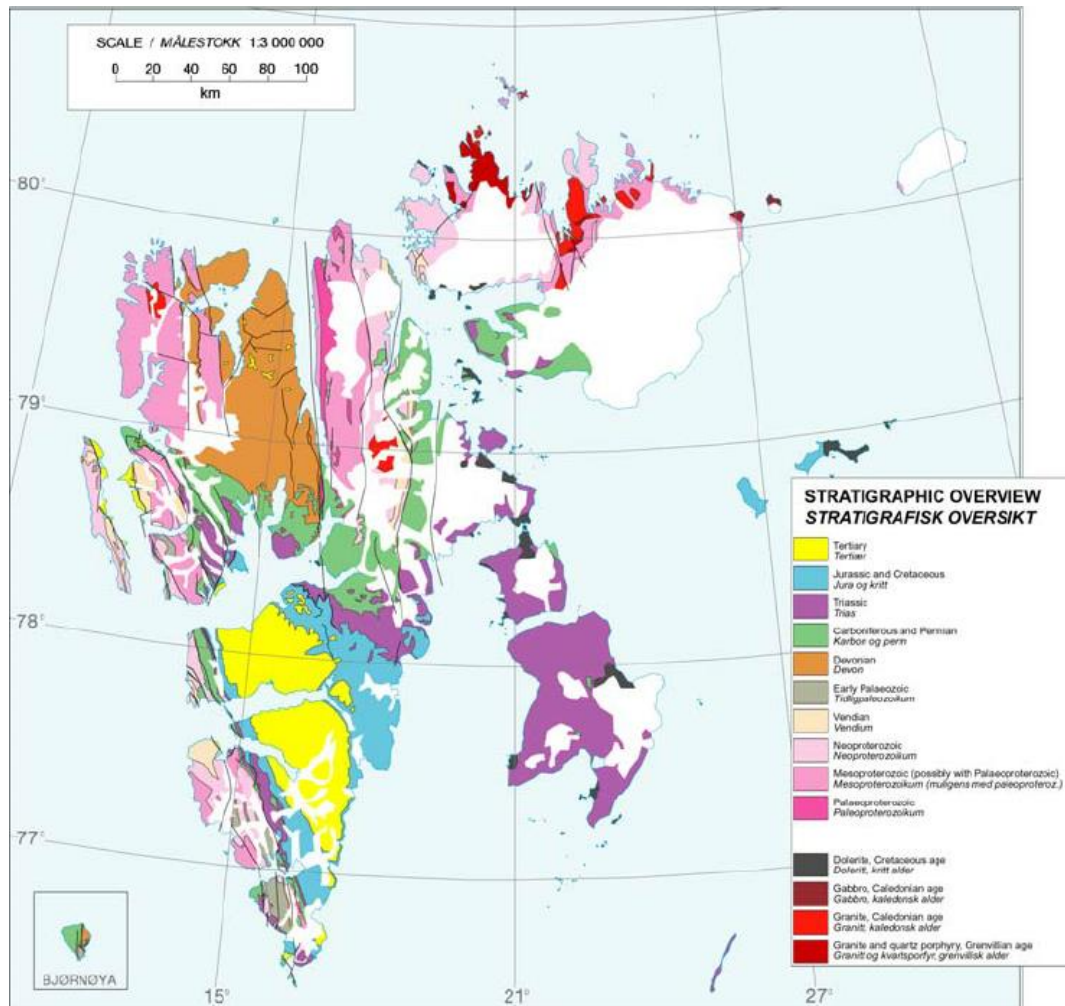


Figure 2.2. Svalbard's geologic regions (Bøggild et al, 2007).

This case study will mainly focus on the island of Spitsbergen, the largest of the islands that make up Svalbard. Spitsbergen contains all of the permanent inhabitants of Svalbard, with the capital, Longyearbyen, located roughly in its geographical center (figure 2.3). The area around Longyearbyen is mainly comprised of coastal lowlands and glacial valleys. Glaciers have greatly impacted the geology and environment on Spitsbergen. These glaciers are cold-based, meaning they are frozen to their beds, or polythermal, meaning they contain both temperate ice at 0°C and cold ice below 0°C (Benn and Evans, 2014). Glaciers nourish groundwaters near the coast and create the valleys found throughout Spitsbergen. This thesis will focus on the central area of Spitsbergen, which is called Nordenskiöld Land. This is a peninsula with the settlements of Longyearbyen, Barentsburg, and Sveagruva. Nordenskiöld Land has tertiary lithology, and is mainly composed of sandstone and shale with many coal deposits. Human habitation has mainly

existed in this area due to the coal fields that have been mined since the early 20<sup>th</sup> century, so data on this region dates back to the early 1900s. Coastal valleys at low elevation on Nordenskiöld Land are of interest because they are where most pingos (see description below) occur on the island.



Figure 2.3. The Svalbard archipelago with settlements on the island of Spitsbergen (Norwegian Polar Institute, 2016). Nordenskiöld Land on Spitsbergen is the peninsula found within the boundaries of the black box.

## 2.3 Historical Glaciation and Climate

In Svalbard, there is a direct link between climate patterns and the mass balance of ice sheets and glaciers. Svalbard was entirely covered by an ice sheet during the Weichselian

glaciation in the Quaternary period, the last glaciation in northern Europe. The ice sheet covering Svalbard and its shelf area was known as the Svalbard-Barents ice sheet (figure 2.4), and it depressed the entire archipelago. The ice sheet began declining around 15 000 years ago via iceberg calving, but a fraction of the ice sheet persisted until about 11 000 years ago when rapid deglaciation followed the Younger Dryas glacial readvancement (Matsuoka et al, 2004). Since the reduction of the ice sheet at the end of the glaciation, Svalbard has been subject to isostatic rebound. During the past 11 000 years, Svalbard has risen approximately 130 meters due to isostasy and continues to rise (Ingólfsson, 2011). Shells can be found on former marine terraces on Svalbard's coastline as evidence that they were once submerged. Although glaciation in the Holocene is at a lesser extent than during the Last Glacial Maximum (LGM), Svalbard's current landscape is largely shaped by the actions of glaciers. The ice sheets eroded fjords and wide U-shaped valleys, particularly in the northern and eastern regions. Svalbard's very thin soil cover was mostly formed during the Quaternary period from erosion and glaciation (Hjelle, 1993). The coastal plains, marine terraces, and other regions that now form part of the Holocene marine limit have saline sediments.

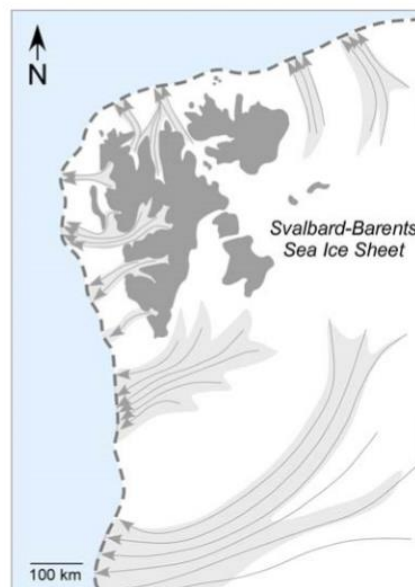


Figure 2.4. The Svalbard-Barents ice sheet during the LGM with ice streams denoted by arrows (Ingólfsson, 2011).

Data on glaciers worldwide was limited prior to the 19<sup>th</sup> century, but Svalbard even more so due to its geographic isolation. No measurements were taken until official scientific expeditions were mounted beginning in the late 19<sup>th</sup> century. Temperature was observed

extensively in western Spitsbergen starting in 1898 and was compiled into a composite series extending between 1898 and 2012 (Nordli et al, 2014). However, these observations are not continuous. The data will often have gaps from the moving of stations and settlements in the early 20<sup>th</sup> century as well as events such as World War II. Although this data is not complete; it is vital for understanding the behaviour of glaciers during the Little Ice Age. The Little Ice Age (LIA) was a climate phenomenon that greatly affected Northern Europe as well as the High Arctic (Hjelle, 1993). The LIA ended approximately before 1918, resulting in slightly warmer temperatures throughout northern Europe and Svalbard. This coincided with an observed reduction in the mass balance of glaciers throughout Svalbard over the past century (Hambrey et al, 2005). It can therefore be argued that climate patterns are among the most important factors in glacier mass balance. In a glacier-dominated landscape such as Svalbard, receding glaciers can have many effects. These include terrestrial erosion rates and changes to the sediment loads added to the surrounding fjords. In turn, benthic communities in the fjords of Svalbard can be affected, changing the dynamics of marine ecosystems (Lønne and Lyså, 2005).

## 2.4 Current Climate Trends

For the purpose of this research paper, climate data from Longyearbyen was used. Longyearbyen is found on the western coast of Spitsbergen. The town is defined as having an ET (tundra) climate using the Köppen Climate Classification System (Eckerstorfer and Christiansen, 2011) because the warmest month on average is between 0°C and 10°C. However, it is important to note that temperatures widely vary across Spitsbergen due to the variation in elevation, proximity to the sea, and oceanic currents (Nordli et al, 2014). Although designated as a polar climate due to its high latitude, Svalbard sees warmer average temperatures than other places at similar latitude such as northern Russia and Greenland (Christiansen et al, 2013). This moderate climate is due to the West Spitsbergen Current that brings warm water from the North Atlantic (Nordli et al, 2014). The seas around western Spitsbergen are navigable and ice-free year-round, particularly when compared to other polar regions. Conversely, the East Spitsbergen Current originates from the Arctic Ocean and brings very cold water. The eastern coast of Spitsbergen is thus much colder and ice-covered than the western side (Aagaard et al, 1987). Because cold and warm air meet at Spitsbergen, this creates very high wind speeds in the winter. Precipitation falls year-round but in small amounts, averaging about 177 mm per year (Norwegian Meteorological Institute, 2011). Svalbard also has the phenomenon of polar days and polar nights. From

November to February, the sun does not rise, and from May to August, the sun does not set (figure 2.5). As a region in the High Arctic, Svalbard is very sensitive to climatic changes such as the phenomenon of polar amplification. This climate sensitivity was highlighted in the IPCC's fifth report (Aas et al, 2016).

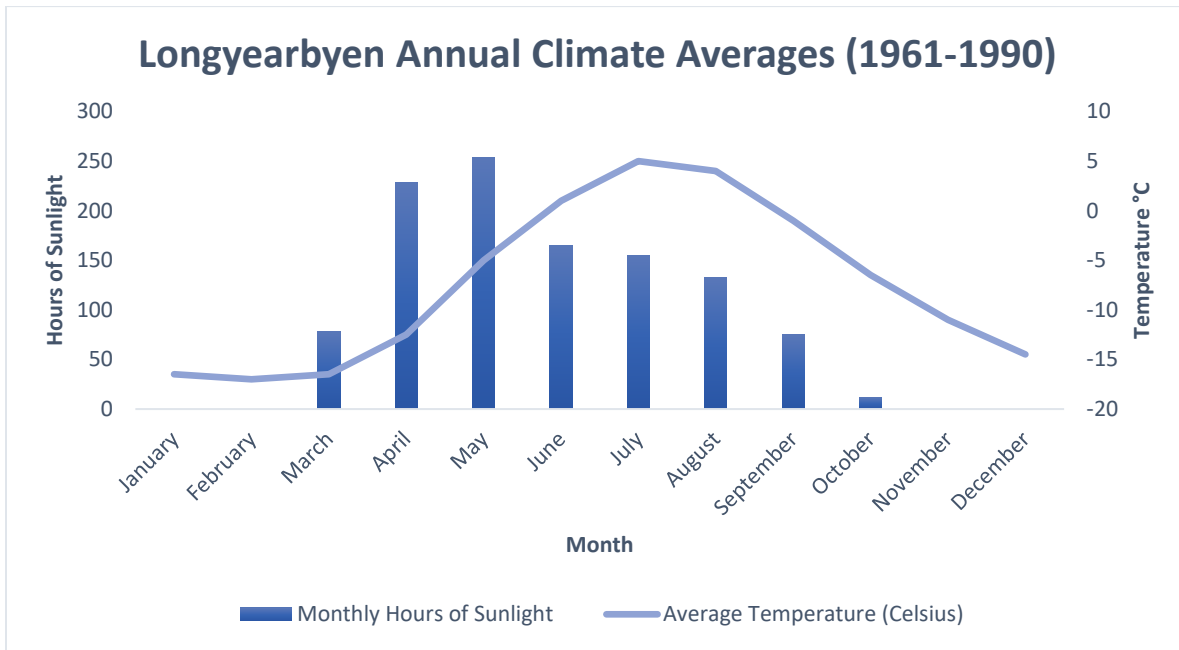


Figure 2.5. Historical average annual temperatures in Longyearbyen and hours of sunlight received. This figure was created using data from the Norwegian Meteorological Institute (2011).

Warming in the Arctic has become a recognized issue worldwide. Svalbard is sensitive to climate differences due to polar amplification. Changes in the net radiation balance produce larger changes in temperature near the poles than in tropical or temperate latitudes (figure 2.6). The result is that the present warming of the Arctic is estimated to be twice that of the global average. Reduced sea-ice cover leads to less albedo, creating a positive feedback of increased warming. Furthermore, moist and warm air masses are carried northward towards the Arctic (Voiland, 2013). This can increase precipitation, mostly in the form of rain rather than snow. As a result, increased warming is most pronounced in the winter season. Temperatures can increase by as much as 10°C in the winter while only increasing by 1°C in the summer. As a polar desert, Svalbard has little annual precipitation. An increase in rain rather than snow cannot maintain glaciers and snow cover (Hansen et al, 2014).

Warmer temperatures recorded in the past thirty years are the likely cause of glacier recession in Svalbard, and continued warming climate trends will most likely exacerbate the loss of mass balance. Moholdt et al (2010) found that small glaciers in Svalbard, particularly those at low elevations, have experienced the highest loss of mass balance. This effect is most pronounced in western Spitsbergen, which overall has warmer temperatures than the east. Glaciers rely on accumulation from winter precipitation in order to maintain a positive mass balance. Although precipitation will increase, this will be in the form of rain and not snow. Without enough accumulation to recover their mass in winter, it is likely that glaciers will experience increased recession rates. Increased recession will affect the hydrology and drainage of Svalbard, which in turn will influence permafrost (van Pelt et al, 2016). The Arctic has natural climate variability and anomalies that occur outside of climate change. It is important to research these natural fluctuations to provide a more comprehensive understanding of how the Arctic environment will respond to a warming climate.

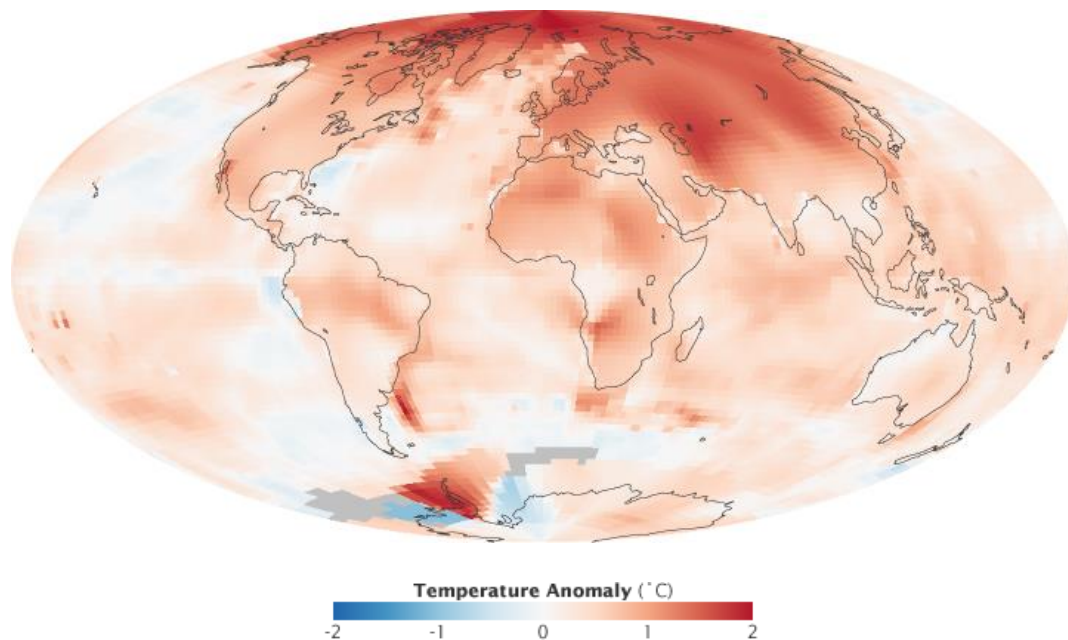


Figure 2.6. Global temperature anomalies from 2000-2009 compared to the global annual mean in the past 50 years. This was created with GISS surface analysis (Voiland, 2013).

### 3. Literature Review

#### 3.1 Glaciers

A glacier is a persistent body of dense ice formed over centuries of snow accumulation that is massive enough to flow under its own weight. Glaciers are a major component of the physical geography and hydrology of Svalbard. Glaciers are not understood as a physical object but more as a system. They gain and lose water and debris. They contribute to the volume of oceans via eustatic sea level rise as well as the atmosphere. Glaciers have an ablation zone, which is defined as the part of the glacier that experiences melting, breakage, and evaporation. Conversely, the accumulation zone is where snow and ice gather. These gains and losses are collectively referred to as the mass balance (Benn and Evans, 2014). Glaciers have historically formed where the accumulation of snow and ice could match or exceed the loss of snow and ice. This naturally means that glaciers are associated with regions of high latitude as well as high altitude where air density and a low solar angle result in low average temperatures and high snow accumulation. They are irrevocably linked with eustatic sea level rise due to their ability to store enormous volumes of ice (Ingólfsson, 2011). Glaciers have eroded the many fjords and valleys found throughout Spitsbergen. The islands of Spitsbergen, Kvitøya, and Nordaustlandet are almost entirely glaciated. The few areas that are seasonally ice-free have evidence of past glacier activity such as moraines. Glaciers have shaped the geomorphology of Svalbard by scouring out massive channels and glacial valleys and by depositing sediment and till. Spitsbergen has valley glaciers as well as ice caps, which are areas of ice smaller than 50 000 km<sup>2</sup> (Pälli et al, 2003).

There are three main classifications of glaciers- temperate, cold, and polythermal (Benn and Evans, 2014). Temperate glaciers are defined by being relatively warm, usually at or near 0°C. They require high precipitation to combat melting rates in summer. Cold-based glaciers have temperatures that are significantly lower than 0°C and are generally frozen to their beds. The type of glaciers found on Svalbard cold-based and polythermal. A polythermal glacier is the most common type of glacier geographically and contains a mixture of temperatures. Different parts of the glacier are below or at the melting point. The temperature of a glacier determines whether or not there is liquid water at the bed and if meltwaters can access or exit the glacier interior without refreezing (Wadham et al, 1998). Spitsbergen has polythermal glaciers which behave in a specific manner due to the polar marine climate. In spring, temperate ice is created in

the accumulation zone when meltwater is refrozen. In the ablation zone, freezing temperatures in winter create a near-surface layer of cold ice. The glaciers found on Spitsbergen have cold as well as temperate ice (Hodson and Ferguson, 1999).

Many of Spitsbergen's coastal areas were once submerged beneath the Arctic Ocean. These areas have now lifted above sea level due to the phenomenon of isostatic rebound. The weight of an ice sheet can depress the earth's crust beneath it. During the Last Glacial Maximum (LGM), the massive weight of glaciers deformed the asthenosphere below Spitsbergen. Many lakes, such as Vårfluesjøen in the north of Spitsbergen, were once marine environments. The shells of prehistoric marine fauna found in these freshwater lakes strongly supports this theory (Røthe et al, 2018). During the LGM, Svalbard was connected with the rest of Europe because of the Scandinavian Ice Sheet. Over the past 8000 years, isostatic rebound in Svalbard has outpaced eustatic sea level rise (Wallmann, 2018). Isostatic rebound rates are not uniform in Svalbard (Bondevik et al, 1995).

### 3.2 Pingos

A pingo is a type of periglacial feature that consists of a core of massive ice with layers of sand and gravel (Yoshikawa, 1993). It appears as a mound or hill that can be ten to forty meters in height and may have a cratered top containing liquid water in summer. Although pingos can be conical, they often have oblong, irregular shapes (Liestøl, 1996). Pingos are traditionally classified into two different forms- open-system, or hydraulic, and closed-system, or hydrostatic. Hydraulic pingos are generally found in continuous permafrost while hydrostatic pingos are features of discontinuous permafrost (Burr et al, 2009). Open-system pingos are the most common type of pingo on Svalbard. Hydraulic pingos develop when groundwater that is under artesian pressure reaches the surface (Müller, 1959). In general, they occur as isolated features or as small groups within the same locality. They generally form in areas with topographic relief, such as lower hillslopes, alluvial fans, or valley bottoms. Groundwater seepage causes icings to form on their domes or at their flanks, which are most visible in late winter (French, 2007).

On Svalbard, many of the larger pingos are related to geologic faults that facilitate the transport of ice melt from glaciers (Liestøl, 1976). This theory is corroborated by studies done on pingos in China (Burr et al, 2009). A discontinuity in the bedrock allows for better transport of

groundwater (figure 3.1). The presence of groundwater can influence the formation of permafrost features such as pingos. Hydraulic pingos grow from ice injection of groundwater from artesian pressure, and three variables are very important to maintain their form. Pingos that are cut off from a supply of groundwater will eventually collapse, such as pingos in Reindalen, Svalbard. Water pressure, which is determined by conditions external to the pingo, overburden strength, and rate of freezing, which depends upon temperature (Yoshikawa and Harada, 1995). Since all three may change independent of the others, this balance will rarely be maintained for the total growth period of a pingo. This is likely why pingos are not common permafrost features.

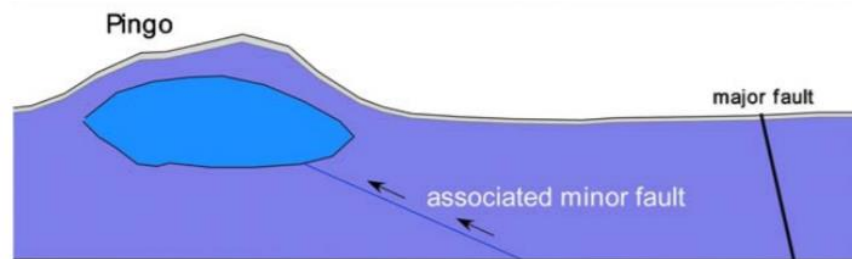


Figure 3.1. Schematic of a pingo in Kunlun Mountain, China, located near South Kunlun Fault and its associated minor fault line (Burr et al, 2009).

### 3.3 Permafrost

On land, pingo growth is associated with the aggradation of permafrost. Permafrost refers to a thermal state when a feature remains at or under  $0^{\circ}\text{C}$  for two years or more (Osterkamp, 2005). Permafrost can contain ice, but it is not defined by the presence of ice because it can occur in ground that does not contain any water. The presence of permafrost influences the population diversity of flora and fauna in Arctic and sub-Arctic environments as well as greatly impacting carbon storage and hydrology. Permafrost makes up a significant part of the physical geography of Svalbard as well as Russia, Canada, China, Mongolia, Alaska, and some parts of Antarctica. Permafrost can exist underneath the ocean and can also be found at high altitudes, such as in the Andes Mountains (Hong et al, 2017). There are four types of permafrost distribution- continuous, discontinuous, sporadic, and isolated. This defines areas that are nearly or completely underlain by permafrost (90%-100%), widespread regions underlain by permafrost (50%-90%), partial coverage (10%-50%), and areas where permafrost only exists in isolated patches (0%-10%) (Brown et al, 1997). Svalbard is underlain by continuous permafrost, as seen in figure 3.1.

Permafrost is well-known for storing high amounts of organic carbon. This is mainly due to the low decomposition rates of organic matter in cold environments. Several studies have described permafrost as a cryosphere cap that prevents or inhibits carbon emissions (Shakhova et al, 2007; Anthony et al, 2012). When permafrost thaw occurs, this organic matter can decompose very quickly and more carbon is added to the atmosphere. Permafrost thaw can also cause issues such as subsidence, which is when the ground collapses because of the loss of volume associated with melting. Frost heave is a similar occurrence that causes ground to expand by up to 9% when water freezes. Permafrost was first described and studied by engineers attempting to reduce the effects of thaw subsidence and frost heave on infrastructure (French, 2007).

Permafrost is a vital component of Arctic geomorphology and hydrochemistry. Permafrost does not exist directly at the surface, where the top layer of soil experiences thawing and freezing cycles associated with seasonality. This layer is known as the active layer, and this is where processes such as microbial activity can occur. Beneath the active layer is a transient layer which is in some years part of the active layer and in some years part of the underlying permafrost (van Everdingen, 1998). Groundwater movement in permafrost can be restricted to the active layer, where seasonal thawing and freezing occur. It can also be restricted to sub-permafrost, unfrozen ground beneath permafrost that can contain deep aquifers (Haldorsen et al, 2010). Within permafrost, there can be unfrozen pockets referred to as taliks. In continuous permafrost, taliks can be created from local heat sources or form following a change in the ground's thermal regime (Ling et al, 2012). Finally, sediments that are saline can be unfrozen below 0°C due to salt water's lower freezing point. In Svalbard, isostatic uplift has exceeded rising sea levels. This means that much of Svalbard's land area was submerged during the Last Glacial Maximum approximately 11 000 years ago and thus contains salty sediments (Elverhøi et al, 1995).



Figure 3.2. Permafrost distribution in the circumpolar north. Image by Philippe Rekacewicz. Data was used from the International Permafrost Association, 1998. Available on the National Snow and Ice Data Center website ([nsidc.org](http://nsidc.org)).

### 3.4 Arctic Hydrology

Permafrost is an important component of Arctic hydrology. Although the presence of permafrost does not necessarily inhibit the movement of groundwater, it is an important factor in water storage as well as responsible for reducing reaction and dissolution rates. Carbon dioxide, calcites, dolomites, gypsum, and siderites are more soluble at lower temperatures (Woo, 2012). The composition of groundwater largely depends on its origin as well as residence time. For instance, siderites are often found in shale and sandstone, which are a vital part of the tertiary geology of Nordenskiöld Land. Groundwater springs can be saline, brackish, or iron-enriched and acidic. Evidence of groundwater flow in winter can be seen in the form of groundwater icings. Groundwater icings are most visible in late winter (figure 3.2), when the active layer has

been frozen for months and air temperatures are not yet sufficient for melting to occur (Anthony et al, 2012).



Figure 3.3. An example of an icing in Adventdalen, Spitsbergen, Svalbard with person for scale. Photograph taken by Emma Ciric in April 2019.

### 3.5 Methane Ventilation

Pingos are unique to continuous permafrost environments, but are not common structures. They require certain hydrological, elevational, and geomorphological conditions in order to form. Pingo-like features that are associated with the decomposition of methane clathrates have been studied on the ocean floor (e.g. Frederick and Buffett, 2014; Berndt et al, 2014; Forwick et al, 2009). Rather than being driven by ice accumulation, the sediment in places like the Beaufort Sea has been expanded and moved by gases. The warming effect of methane per unit mass is 28 times higher than that of carbon dioxide (Mau et al, 2017). Methane clathrates, used synonymously with methane hydrates, are substances formed when methane gas is forced into a solid form by a combination of high pressure and low temperatures. Methane clathrates are crystalline and can have the same appearance as ice (Portnov et al, 2016). An increase in temperature or decrease in pressure can cause rapid ventilation of methane through the water column and into the atmosphere.

The dissociation of methane hydrates in submarine sediments can be an indication of past climate change. Because the stability of a methane clathrate relies on temperature and pressure, dissociation can be used to study previous variations in ocean conditions (Marín-Moreno et al, 2013). Because so little is known about methane hydrates in the present, this information could be used for present implications of methane affecting the Arctic carbon budget (Westbrook et al, 2009). In Russia, several studies have been done on the link between subsea permafrost and methane hydrates (Serov et al, 2015; Portnov et al, 2013; Portnov et al, 2014). This is because permafrost can act as a seal for methane, one that either traps methane entirely or limits its release. The thaw of coastal and subsea permafrost throughout Svalbard is very likely to affect the natural emissions of methane. Permafrost-associated methane hydrate deposits are found at shallow depths within the sediments of Arctic continental shelves. Frederick and Buffett (2014) found that taliks can provide an escape for methane when dissociation occurs. This temperature anomaly can occur due to hydrological, geochemical, or thermal conditions. On Spitsbergen, taliks have been found beneath open-system pingos (Riedel et al, 2018).

It has been shown in previous studies (Hodson et al, 2019; Portnov et al, 2016) that significant contributions to methane in the atmosphere can be made by methane reservoirs located in or below sub-permafrost ground water. In Nordenskiöld Land, methane can escape via open-system pingos. The creation of open-system pingos has been linked to isostatic uplift and permafrost aggradation as a result of ice sheet retreat since the Last Glacial Maximum. Open-system pingos can also originate from pockmarks on the ocean floor, which act as a conduit for methane escape much like pingos do on land. Pockmarks have similarly been associated with the retreat of the ice sheets since the LGM (Crémière et al, 2016).

### 3.6 Microbes as a Source of Methane

Strong evidence supports microbiological activity as a major source of methane in Svalbard. Compounds converted into hydrogen and carbon dioxide and then reduced to methane are an indicator of microbiological activities. Studies (Müller et al, 2018; Mackelprang et al, 2011; Wagner and Lieber, 2010) have shown that Adventdalen in particular has such a large amount of methane due to particularly high rates of anaerobic microbiological activity. These bacteria form methane in a process known as methanogenesis. Methanogenic archaeobacteria belonging to the families *Methanobacteriaceae*, *Methanomicrobiaceae*, *Methanosarcinaceae*,

and *Methanosaetaceae* (Wagner and Lieber, 2010) have been identified in Arctic permafrost environments. Adventdalen has been the valley that has been studied most in Svalbard, due to its proximity to the capital of Longyearbyen and thus ease of access. It is possible that methanogenic archaea are the source of methane that is emitted in other valleys such as Reindalen and Grøndalen. As these microbes are most active during the thaw, it can be estimated that their activity will increase if temperatures warm. However, little is known on the current population and the density of existing methanogenic archaea in Svalbard.

## 4. Materials and Methods

### 4.1 Cartography

Using topographic maps of Svalbard provided by the Norwegian Polar Institute (2016), pingos were identified throughout Svalbard to create a database. Pingos are visible on satellite imagery as singular or grouped craters or hills on lowland terrain. A map of all pingos found in coastal lowlands across Svalbard was created using QGIS and Sentinel satellite imagery provided by the Norwegian Polar Institute (2016). Lowlands are parts of Svalbard that are light brown in maps (figure 2.1), generally in the form of valleys and coastal plains. Pingos were located using topographic maps. Icings were located using winter satellite imagery. Icings that appear in late winter are indicative of pressurized groundwater. These icings can be associated with mountain springs, glaciers, or pingos.

Although pingo icings were located across the island of Spitsbergen, the geographic focus was on the peninsula of Nordenskiöld Land on the island of Spitsbergen because of the quantity of pingos and ease of access for field work. Icings of mountain spring and glacial origin were denoted on Nordenskiöld Land. In addition to locating icings, fault zones were mapped across all of Svalbard. Faults occur frequently and in large clusters across Spitsbergen, particularly in areas associated with pingos. The distance between pingos and the nearest fault line was measured to find an association between the two features.

It is hypothesized that thicker marine infill at the Holocene marine limit allows for less groundwater passage because of low permeability. Essentially, groundwater is forced out the sides of the valley where the marine infill is thinner (Røthe et al, 2015). Based on this hypothesis, pingos should be found at the valley margins in the Holocene marine limit and closer to the center outside of this limit. To achieve this, distance was measured between the pingo and the center of the valley. This distance was then divided by the total width of the valley in order to obtain a 0-1 index for proximity of the pingos to the valley center, with 0 being near the margins and 1 being at the center.

## 4.2 Sampling in the Field

Field work was completed from March to May 2019 with visits to wide glacial valleys on Nordenskiöld Land. Data collection was completed over three months. Field sites were chosen based on the locations of icings found on satellite imagery. Many of these sites have been sampled in previous studies (Hodson et al, 2019). The purpose of these visits was to make observations of the presence of pingos previously identified on satellite imagery, or other features with methane seepages such as pro-glacial groundwater icings. Well-known, active pingos that have been well documented in literature (Yoshikawa and Harada, 1995; Liestøl, 1977) were visited as well as new icings. Snowmobiles and boats were used to reach the field sites as well as for transferring materials back to the University Centre in Svalbard. Camping supplies in case of emergency always accompanied the snowmobiles. The following factors were measured: gaseous methane, carbon dioxide, oxygen, electroconductivity, PH, and oxidative-reductive potential.

The purpose of sampling in valleys in Spitsbergen was to check for methane evasion using a headspace methane detector. Sites were selected based on the presence of groundwater icings. Icings were located using winter satellite imagery from the Norwegian Polar Institute (2016) with a resolution of 1:15 000. A Panasonic power drill was used to pervade the ice and allow the liquid water to escape. Water that was not pressurized and did not rapidly spout from the core was not measured, as this indicated standing water that was not near the source. Three syringes were filled with water directly from the drilled core and passed into a flow cell. The flow cell was heated to prevent freezing and had four membrane detectors to analyze pH, electrical conductivity, oxidation-reduction potential, and dissolved O<sub>2</sub> (figure 4.1). The detectors were read using a Hach HQ40 multimeter. OxyGuard and Pro Oceanus laser detectors (figure 4.2) were used to measure free carbon dioxide and gaseous methane concentration as  $x\%$  of total gases, respectively. One measurement for each substance was made per station. This information was entered into a field laptop. The elevation, geographical area, geological area, and associated groundwater icings were described and annotated in a notebook. Using the measured data, the distribution of methane concentration throughout Nordenskiöld Land was mapped and compared to known sites.



Figure 4.1. Water from a groundwater icing being passed through membrane detectors. Photograph taken by Emma Ciric in May 2019.



Figure 4.2. A Pro Oceanus laser detector measuring methane parts per million at a glacial spring near Foxfonna Glacier, Svalbard. Photograph taken by Emma Ciric in July 2019.

### 4.3 Statistical Analysis

Mass spectrometry was intended to be completed on water samples taken in winter 2019, but these results were not possible due to mechanical failure. In order to supplement this, data was obtained from previous sampling done in four pingo sites in Adventdalen, Nordenskiöld Land, Spitsbergen (Hodson et al, in review). These pingo sites release very high quantities of methane and thus data from the years 2015 to 2017 has been used to conduct statistical analysis. Measurements from 2015-2017 refer to aqueous methane expressed as mg/l while the samples collected in 2019 (within this thesis) refer to gaseous methane and are expressed as  $x\%$  of the total measured gases.

Using data from the above-mentioned paper, SPSS was used to conduct a factor analysis of correlations between various substances detected in the water at four different sites in Adventdalen between the years 2015 and 2017. The factor analysis was done on winter samplings from Lagoon Pingo, Førstehytta Pingo, Innerhytta Pingo, and River Pingo. The variables used were: methane, carbon dioxide, ammonium, silicate, bicarbonate, chloride, sulfate, sodium, potassium, magnesium, calcium, strontium, iron, manganese, and total dissolved solids. Microsoft Excel was used to form a linear regression for methane at these four sites to identify what components can be used as explanatory variables for methane. Methane was used as the dependent variable with deuterium and carbon dioxide used as independent variables against it.

## 5. Results

### 5.1 Spatial Distribution of Pingos

A total of 98 pingos were found on two islands in Svalbard. The vast majority (92) are on Spitsbergen, the largest island in the archipelago. There were 6 pingos found on the island of Edgeøya. Of the 92 pingos on Spitsbergen, 60 are located on the peninsula of Nordenskiöld Land located at the center of the island (figure 5.1).

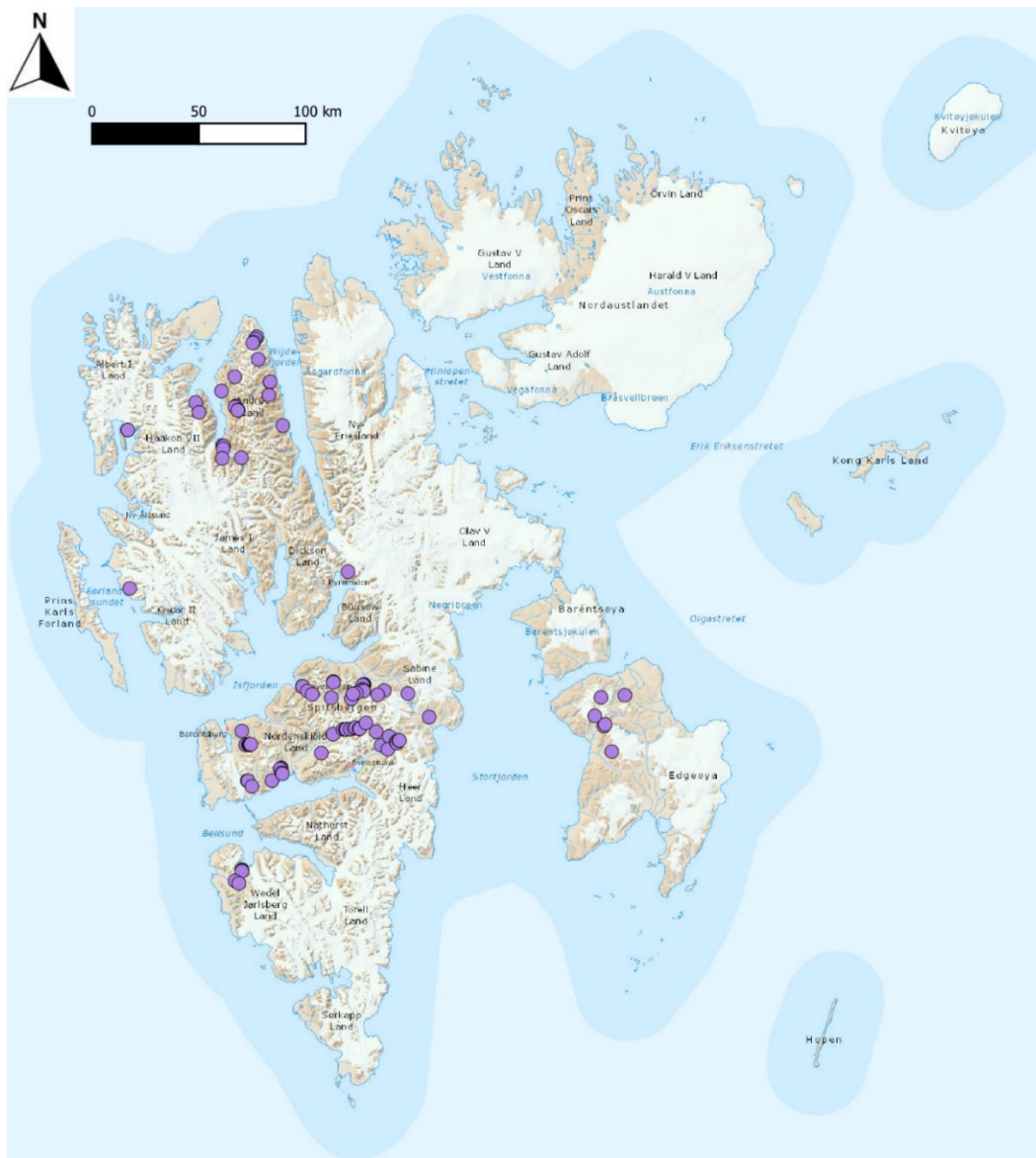


Figure 5.1. Location of all identified (98) pingos (purple circles) at Svalbard. The largest cluster is located on Nordenskiöld Land, in the center of Spitsbergen.

Groundwater icings visible in the winter can have multiple sources such as mountain springs, glaciers, and pingos. Figure 5.2 shows the locations of pingo-associated icings across all of Svalbard. Pingo icings are mainly confined to the peninsula of Nordenskiöld Land in central Spitsbergen. No pingo icings were found on any other islands.

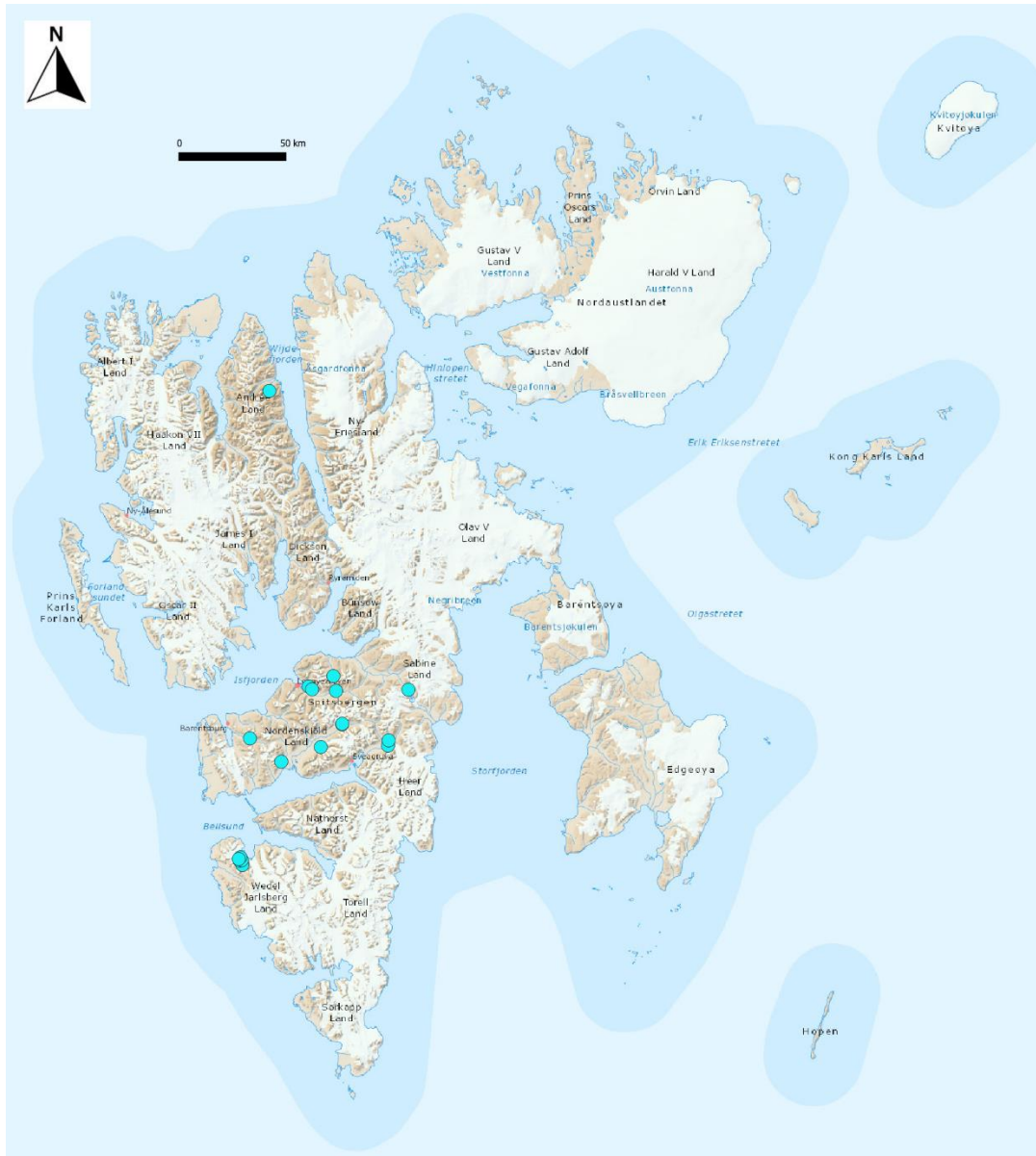


Figure 5.2. Location of pingo-associated icings on Svalbard.

Pingo clusters are found in multiple areas of Svalbard, but only the ones in Nordenskiöld Land have visible groundwater recharge. In Nordenskiöld Land, there are many groundwater icings visible in winter that are not associated with pingos. These icings are typically of

mountain spring or glacial origin. Figure 5.3 shows the locations of all icings derived from pingos, mountain springs, and glaciers on Nordenskiöld Land in central Spitsbergen.

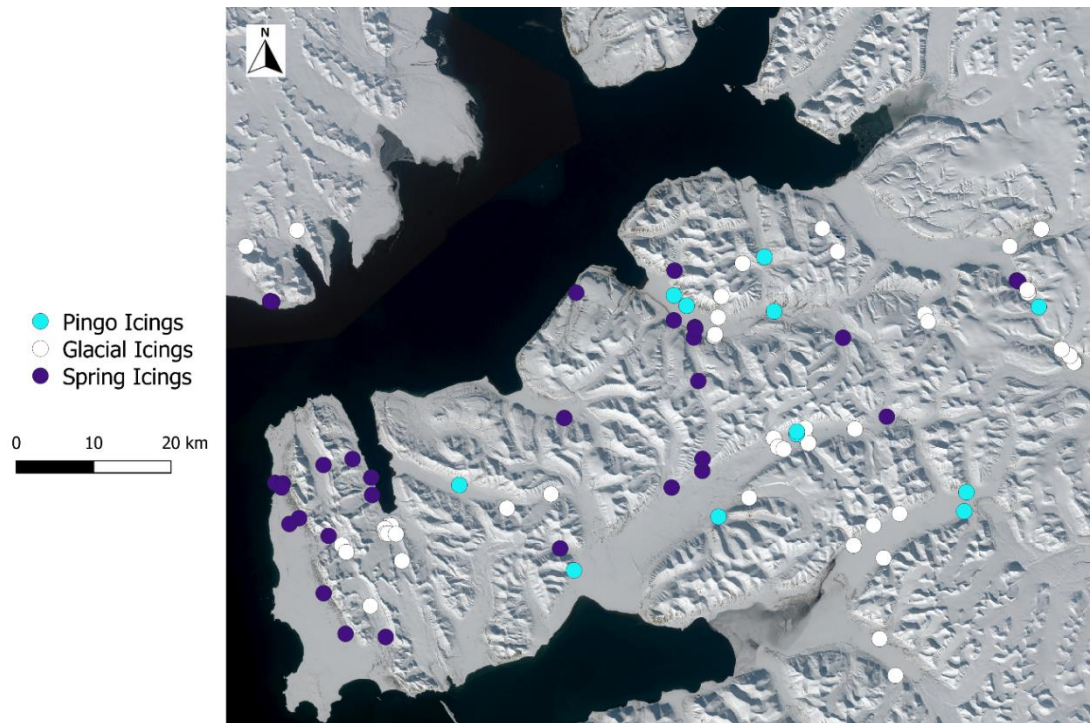


Figure 5.3. Groundwater icings on Nordenskiöld Land. The colour-coding distinguishes what features are associated with the icings.

Pingos are features that only occur at low elevations (figure 5.4). Of the 98 pingos, 67 are located on flood plains or valley bottoms that are at or below 100 meters above sea level. Only one pingo was found above 200 meters, in a valley bottom 213 meters in elevation.

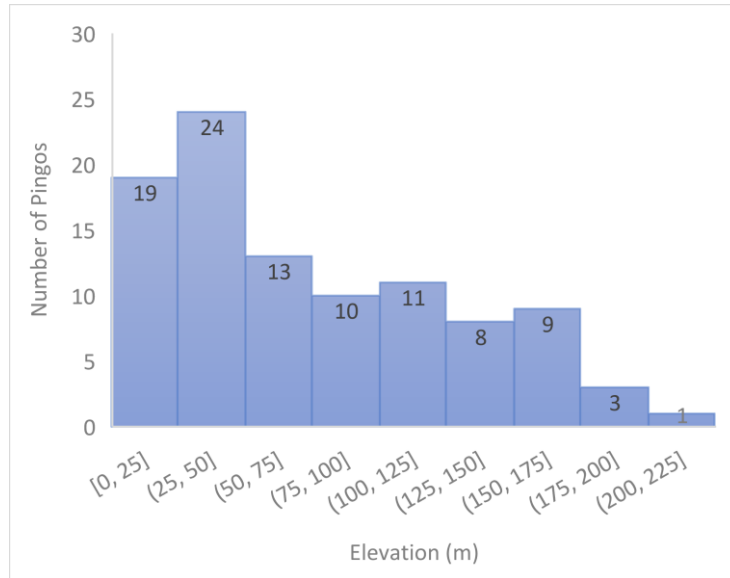


Figure 5.4. Pingo elevations throughout the archipelago of Svalbard.

## 5.2 Methane in Nordenskiöld Land

River Pingo, Innerhytta, Førstehytta, and Lagoon Pingo in Adventdalen (figure 5.5) were the four pingos that were the focus of studies from 2015 to 2017 (Hodson et al, in review). In this paper, aqueous methane was reported in mg/l while. The Lagoon pingo had 59% gaseous methane, River pingo had 7%, and Innerhytta pingo had 15% when sampled in winter 2019. Førstehytta pingo was not sampled in 2019 because there was no visible icing.

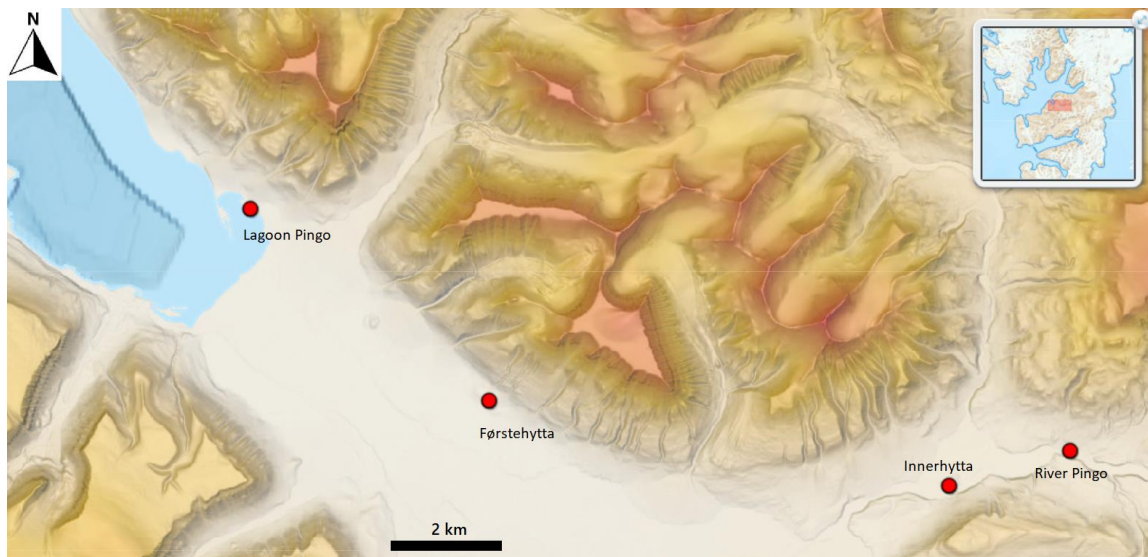


Figure 5.5. The locations of the four pingos sampled between 2015 and 2017 (red circles) in Adventdalen Valley, Nordenskiöld Land, Spitsbergen by Hodson et al (in review).

A total of 20 sites in Nordenskiöld Land were identified and chosen for measurement based on the presence of groundwater. All locations chosen were valleys that had known pingos, terminal glacier moraines, or both (figure 5.6).

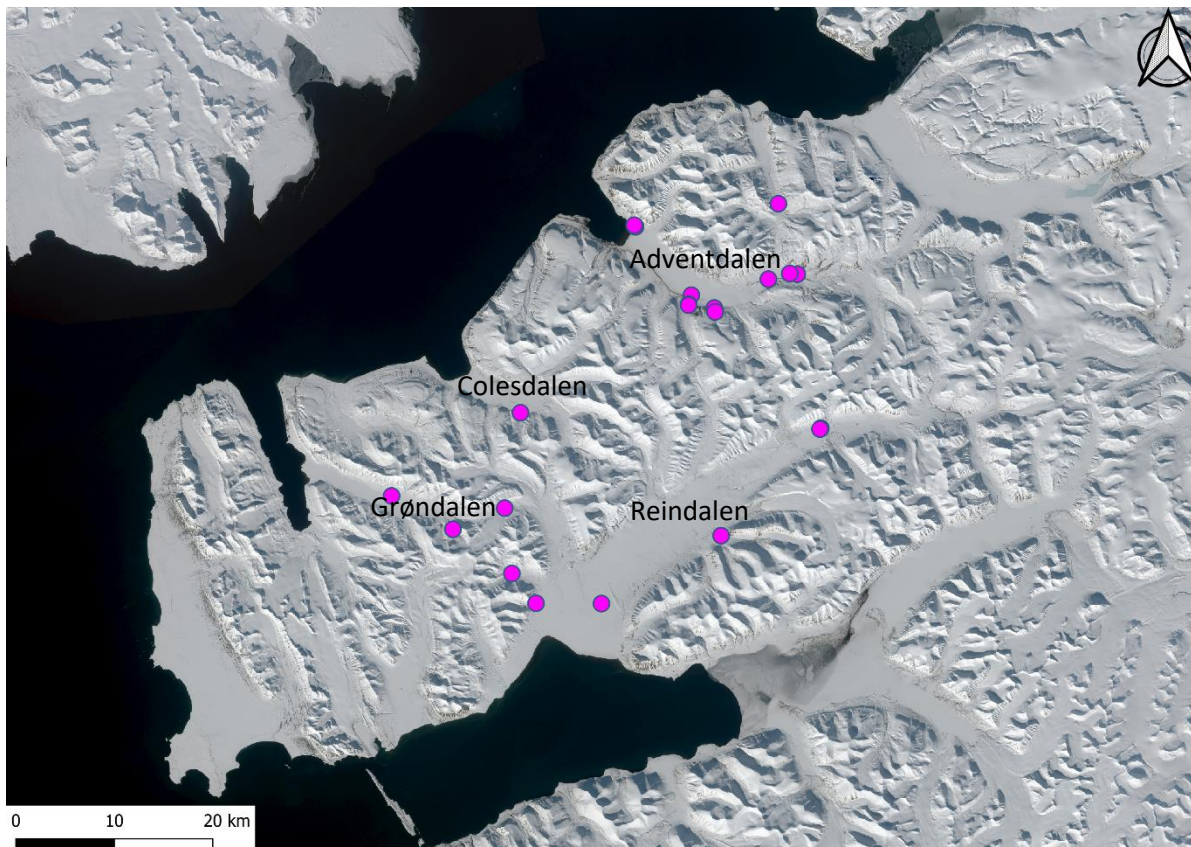


Figure 5.6. The locations of winter sites in Nordenskiöld Land visited in 2019.

Methane was the focus of the compound analysis (figure 5.7). A map was created to show the spatial distribution of different amounts of methane throughout Nordenskiöld Land. Values ranged from 0% to 59% gaseous methane in pingo icings. By far, the highest amounts of methane were in the valley of Adventdalen. Other valleys such as Reindalen and Grøndalen had pingo icings with up to 6% gaseous methane, but most sites with methane in Adventdalen exceeded 10%. Furthermore, only two glacial icings in Nordenskiöld Land had any traces of methane. Both of these values were under 4%.

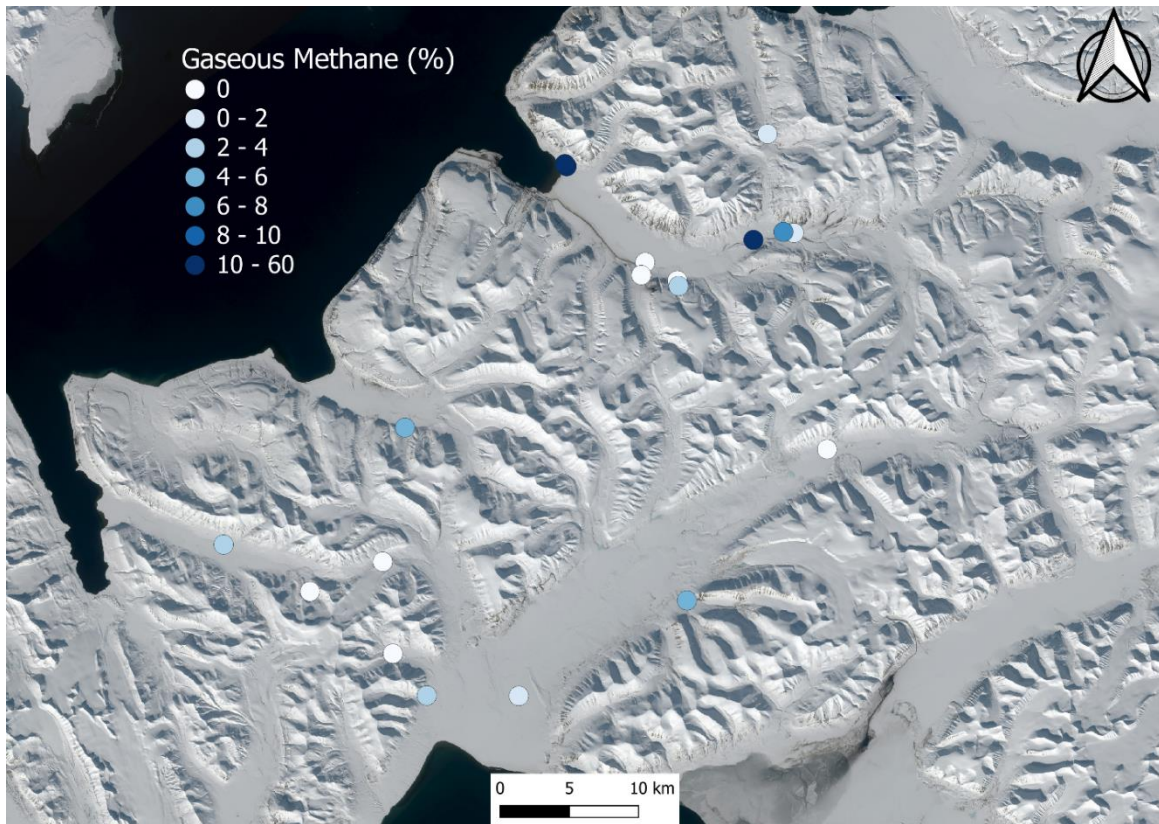


Figure 5.7. Gaseous methane expressed as a percentage of the total gases at sites throughout Nordenskiöld Land. One measurement was made at each site during a sampling period from March to May of 2019.

Of the other components analyzed in winter 2019, free oxygen had the most visible correlation with gaseous methane. Sites that had free oxygen often correlated with low levels of methane (figure 5.8). In the valley of Trodalen, a site had already been drilled prior to study in March of 2019. The water within had equilibrated and become enriched with oxygen, and no methane was detected.

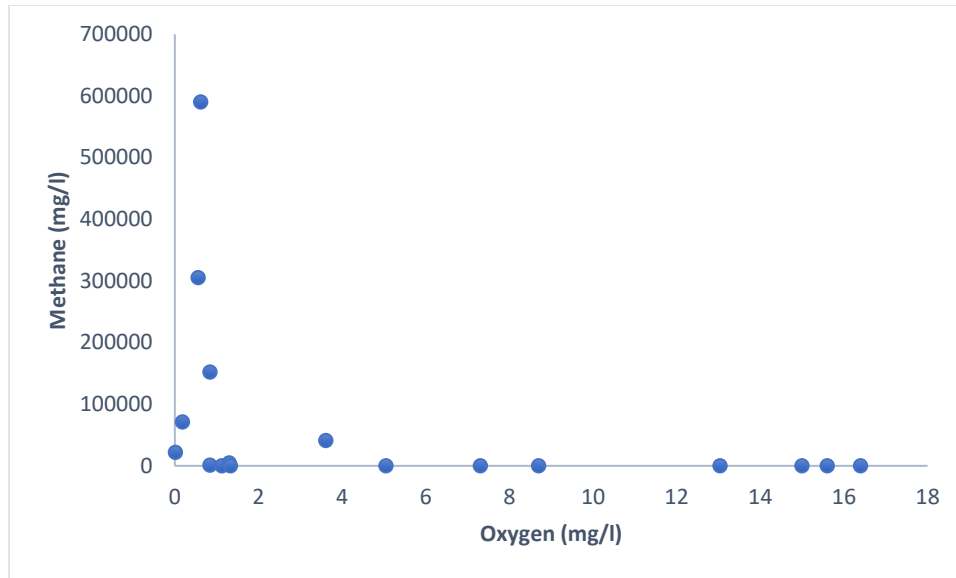


Figure 5.8. Based on data collected in winter 2019 from Nordenskiöld Land, high methane release from icings is generally associated with low oxygen release.

### 5.3 Elements of Pingo Formation

No pingos were found further than 20.4 km away from the nearest fault line on the island of Spitsbergen (figure 5.9). Of the 92 pingos on the island, only 25 were farther than 10 km from the nearest fault line. 31 pingos were one kilometer or less from the nearest fault line. Mean distance was 5.45 km while median distance was 2.98 km. The mean distance is greater than the median distance, which results in data that is positively skewed (figure 5.10). The island of Edgeøya was not included in the analysis or in figure 5.10 because no data on fault lines was found east of Svalbard. Faults exist with high density in Spitsbergen, and in regions such as Andrée Land (figure 5.11) pingos follow the normal fault lines along several valleys. Only one pingo icing was found in Andrée Land. In regions such as Wedel Jarlsberg Land (figure 5.12) and Nordenskiöld Land (figure 5.13), pingo icings were found near reverse fault lines.

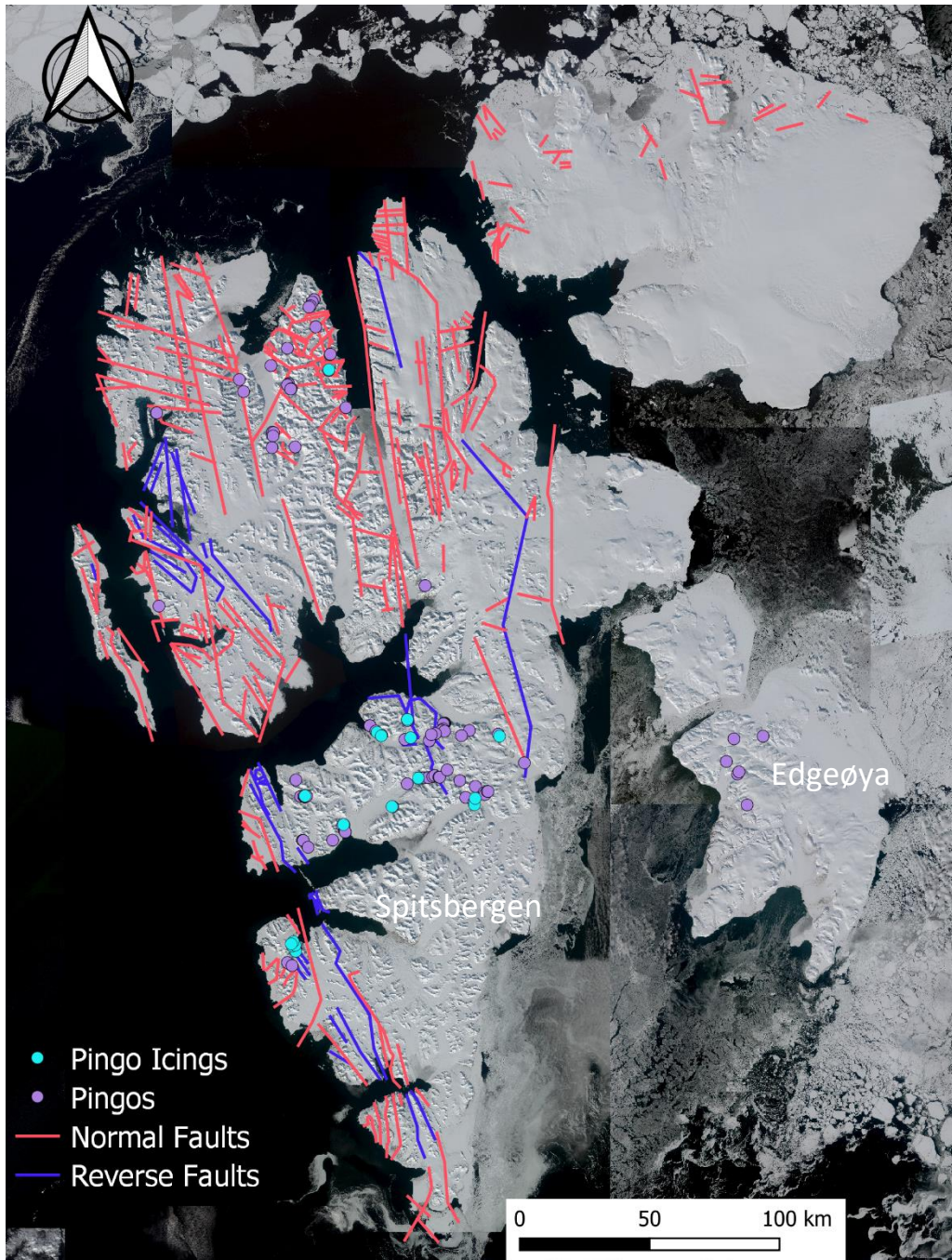


Figure 5.9. Known and assumed normal fault lines on Svalbard (red lines) and reverse fault lines (blue lines) relative to the position of pingos (purple circles) and pingo icings (blue circles) on Edgeøya and Spitsbergen.

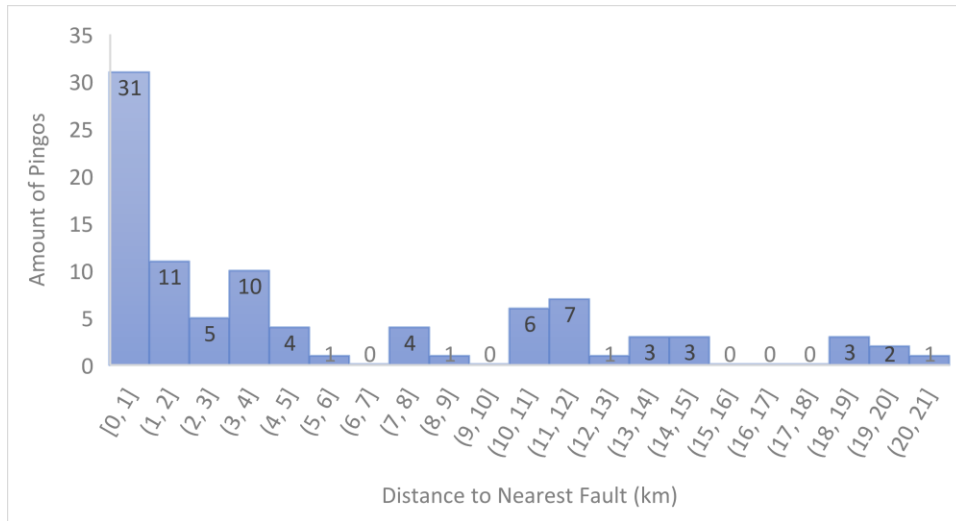


Figure 5.10. Distance of pingos on Spitsbergen to the nearest fault in kilometers. The island of Edgeøya was not included due to the fact that there is no geological data east of the island.



Figure 5.11. In André Land, pingos (purple circles) are closely aligned with or nearby normal fault lines in red.

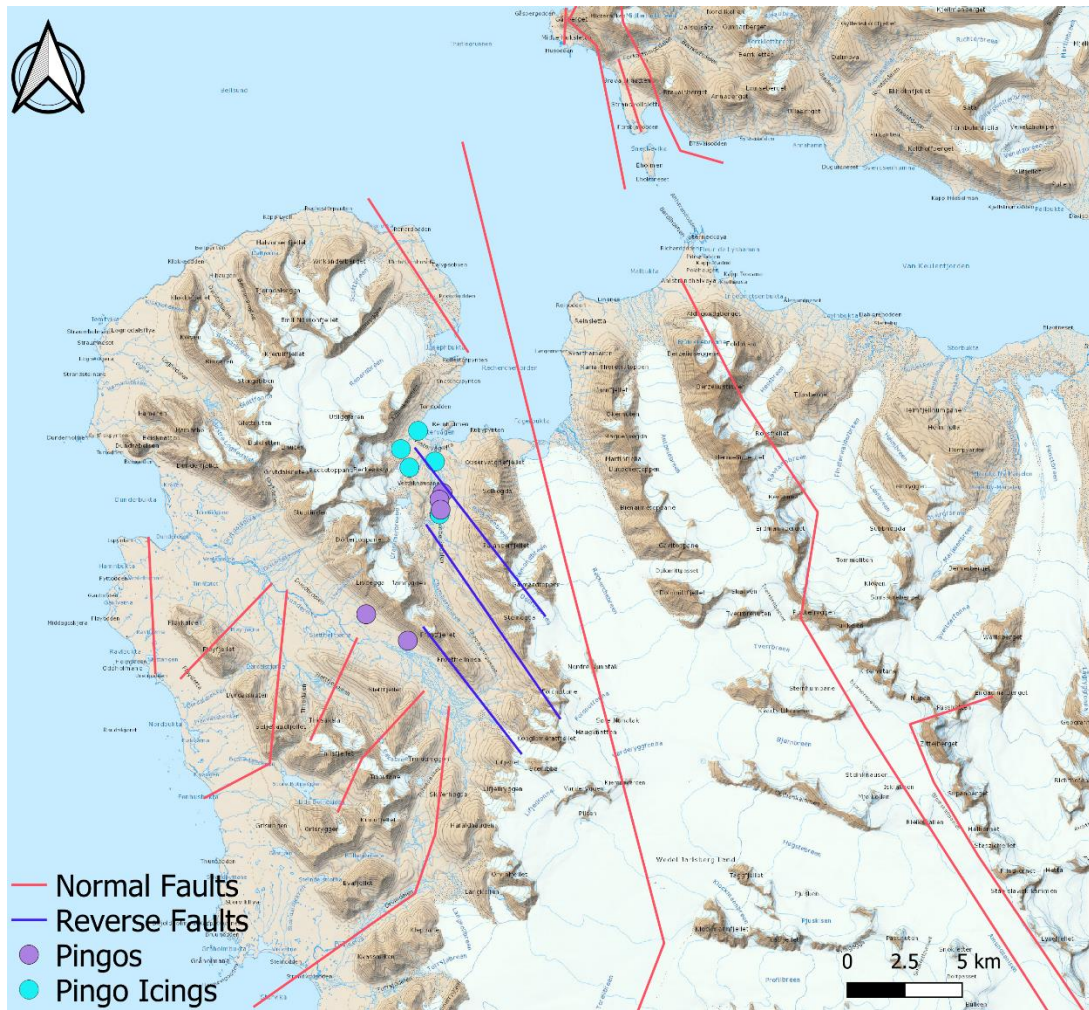


Figure 5.12. Relationship between pingos (purple circles) and pingo icings (blue circles) relative to normal faults (red lines) and reverse faults (blue lines) in Wedel Jarlsberg Land, Spitsbergen.

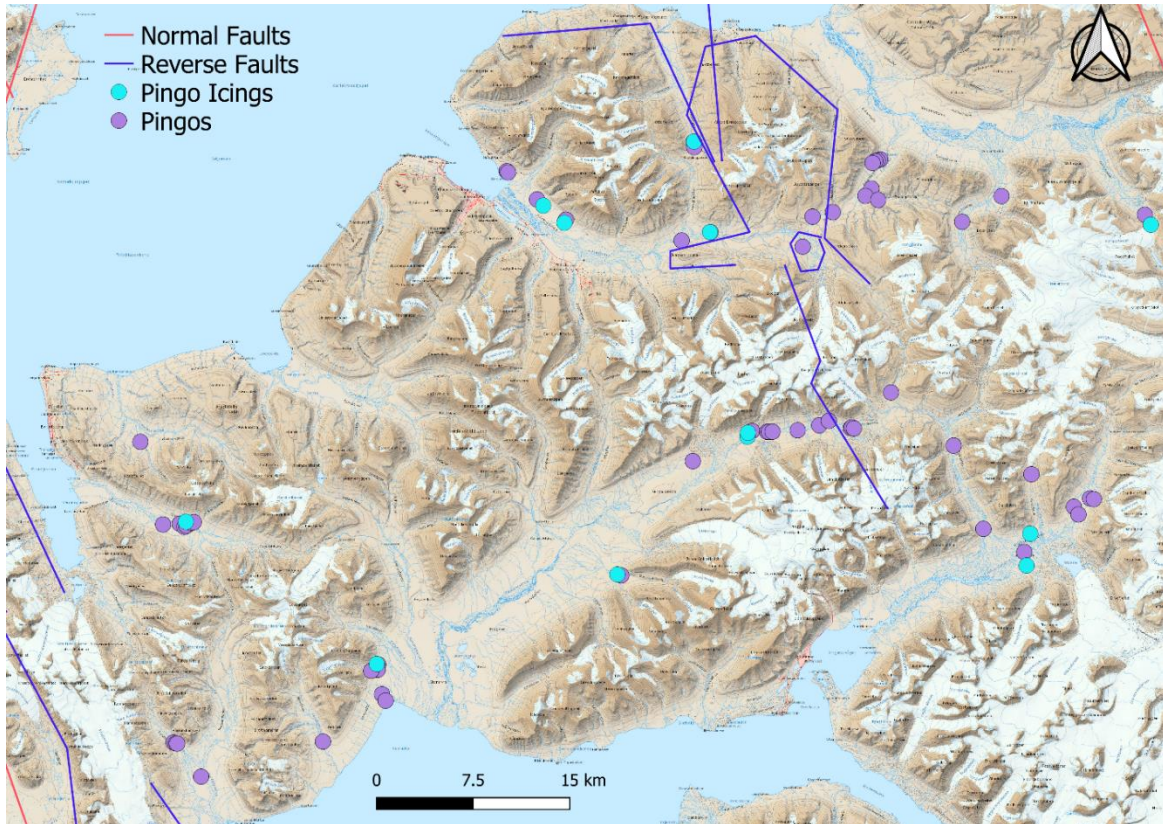


Figure 5.13. Relationship between pingos (purple circles) and pingo icings (blue circles) relative to normal faults (red lines) and reverse faults (blue lines) in Nordenskiöld Land, Spitsbergen.

Pingos being found at the valley margins closer to the marine limit and at the center of the valleys farther from the marine limit only occurred in a few regions (figure 5.14). The distribution of pingos across the valleys is slightly bimodal, but the peaks are not distinct enough to be significant (figure 5.15).

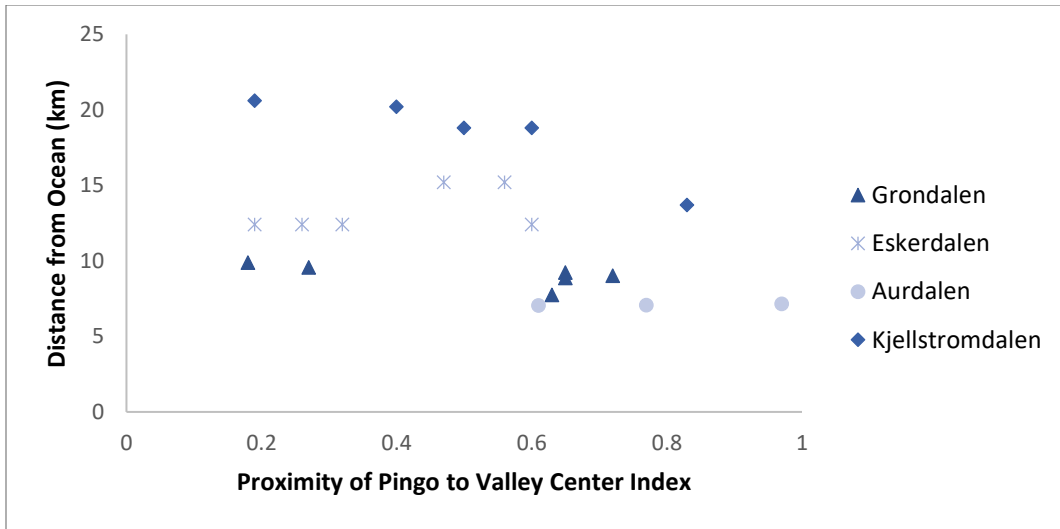


Figure 5.14. Example of four pingo groups in valleys on Svalbard and their proximities to the valley center. On the index, 0 is the valley margins while 1 is the exact center of the valley.

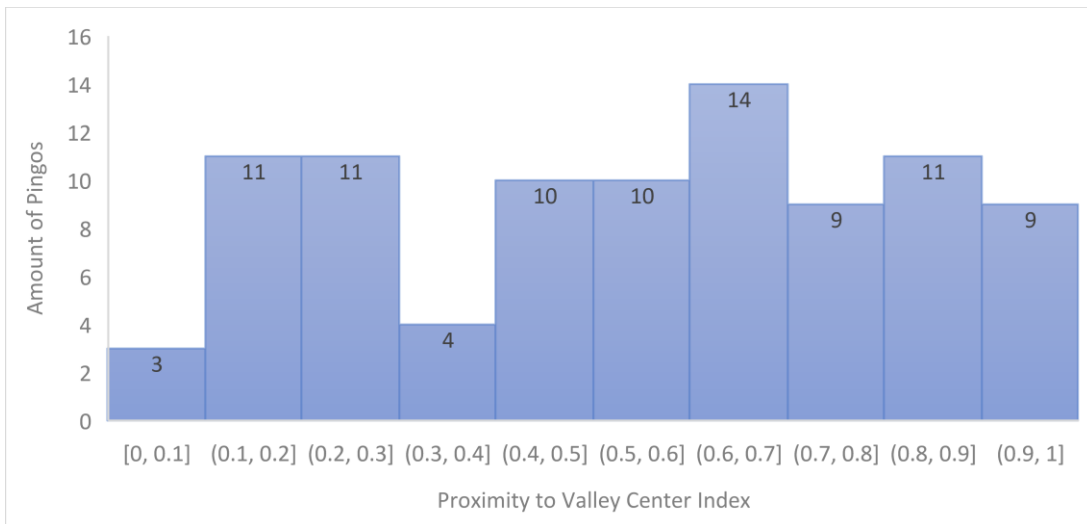


Figure 5.15. Index of pingos relative to their position in the valleys, with 0 being as close as possible to the sides of the valley and 1 being as close as possible to the center of the valley.

## 5.4 Relationship Between Methane and Other Compounds

Principal component analysis was used to reduce the dimensions of the 2015-2017 dataset (Hodson et al, in review) and facilitate interpretation of the dominant factors linked to methane. The SPSS analysis of winter data sampled between 2015 and 2017 permitted the identification of four major components that justify correlations between different substances in the groundwater. Four factors were retained on the basis of their eigenvalues being greater than

1. As a consequence, four components were retained that described  $x\%$  of the total variance in the dataset. Each major component justifies the relationship between certain elements and compounds (table 5.1). In component 1, carbon dioxide and methane appear to be closely correlated with values of 0.72 and 0.70, respectively. In component 2, total dissolved solids are strongly associated with sodium and with bicarbonate. Component 3 explains the association between ammonium and strontium, while the fourth and final component is largely responsible for manganese. Component 1 explained 38.7% of the variance, while component 2 explained 29.0% of the variance. Component 3 justified 14.7% of variance, and component 4 was 10.4% of variance. In total, 92.8% of the variance was cumulatively justified by the four components.

Table 5.1. Component analysis of the measured chemical elements, compounds, and total dissolved solids (TDS) from four pingos in Adventdalen, Spitsbergen, Svalbard.

<i>Substance</i>	<i>Component</i>			
	<b>1</b>	<b>2</b>	<b>3</b>	<b>4</b>
<i>CH4</i>	.70	.25	.50	.35
<i>CO2</i>	.72	.43	-.07	.41
<i>NH4</i>	-.27	.12	.86	.34
<i>Si</i>	-.64	-.18	-.63	.28
<i>HCO3</i>	-.24	.92	-.21	-.07
<i>Cl-</i>	.93	.05	.26	-.03
<i>SO4</i>	-.89	.40	.00	.08
<i>Na</i>	.39	.91	-.02	-.09
<i>K</i>	-.96	.20	.07	-.01
<i>Mg</i>	-.72	.63	-.04	.01
<i>Ca</i>	.44	.84	-.22	.04
<i>Sr</i>	.59	-.08	-.72	.26
<i>Fe</i>	.69	-.23	-.29	-.38
<i>Mn</i>	.05	.25	.20	-.92
<i>TDS</i>	.07	.98	-.09	-.02

Deuterium (D) and carbon dioxide (CO<sub>2</sub>) were found to be the most statistically significant when compared against methane (figure 5.16, figure 5.17). The p-values were all very small (table 5.2), indicating that the test was statistically significant. When a multiple regression was done in Microsoft Excel, they accounted for 91.0% of the variance of methane. Originally  $\delta^{18}\text{O}$  was used instead of deuterium because it is generally associated with methanogenesis, but  $\delta^{18}\text{O}$  only justified 87% of the variance of methane. Thus, deuterium was used. The R-squared

value of deuterium and carbon dioxide was 0.910 and the adjusted R-squared value was 0.902. This means that very few variables were not significant. Using this regression, an equation was proposed to estimate methane based on the proportions of carbon dioxide and of deuterium.

Table 5.2. Regression statistics with methane used as the dependent variable and with carbon dioxide and deuterium as the independent variables. All values are significant as they have significance levels lower than 0.05.

	<i>Coefficients</i>	<i>Standard Error</i>	<i>t Stat</i>	<i>P-value</i>
<i>Multiple Regression Intercept</i>	195.1	24.58	7.939	6.70E-08
<i>Carbon Dioxide</i>	0.019	0.004	4.583	1.45E-04
<i>Deuterium</i>	1.758	0.226	7.759	9.75E-08

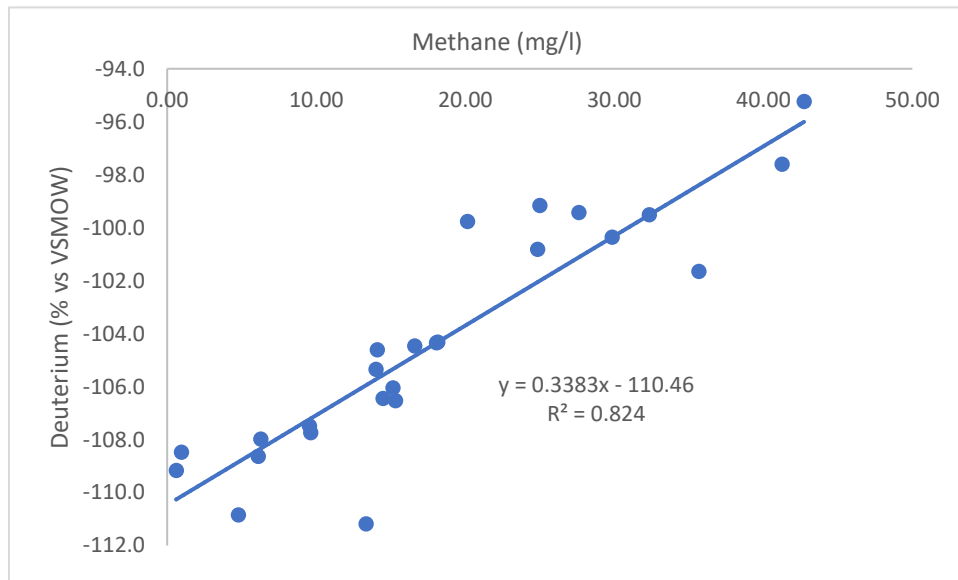


Figure 5.16. Relationship between deuterium and methane based on data from Hodson et al (in review). The methane described here is aqueous methane expressed as mg/l. Significance was 3.78E-10.

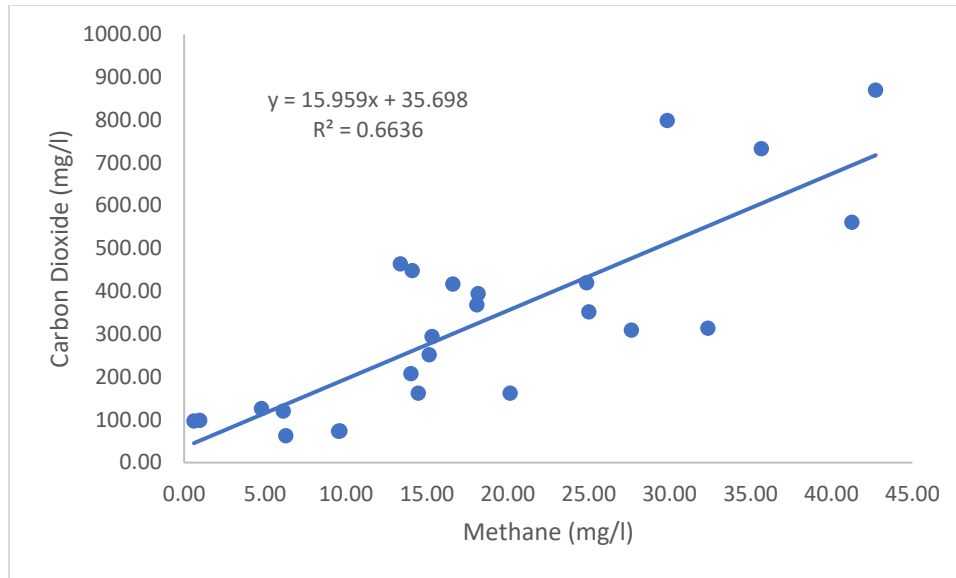


Figure 5.17. Relationship between carbon dioxide and methane based on data from Hodson et al (in review). The methane described here is aqueous methane expressed as mg/l. Significance was 7.19E-07.

Using the linear regression equation  $y = a + bx$  and the coefficients of the intercept, carbon dioxide, and deuterium, the following equation was created as a predictive model for methane concentration based on levels of deuterium and carbon dioxide. The expression  $y_{CH_4}$  is the concentration of dissolved methane in water in mg/l. The variable  $x_{CO_2}$  is the concentration of dissolved carbon dioxide in water in mg/l, and  $x_D$  is a percentage of deuterium compared to VSMOW (Vienna Standard Mean Ocean Water).

$$y_{CH_4} = 195.1 + 0.019x_{CO_2} + 1.758x_D$$

## 6. Discussion

### 6.1 Physical Geography of Pingos on Svalbard

Pingos in Svalbard are only found in terrain that is not glaciated and low in elevation. The highest pingo on the archipelago was found at 213 meters above sea level. Of the 98 pingos, 67 of them were found below 100 meters in elevation. Pingos rely on regular injections of groundwater to exist and thus cannot be found on steep slopes or at high elevations. Pingos that are cut off from groundwater supply cannot develop and are considered inactive (Liestøl, 1996). Furthermore, they cannot exist where there are ice caps or glaciers. Because nearly two-thirds of Svalbard is glaciated, there is a limited amount of land area for pingos to form. All pingos found on the islands of Spitsbergen and Edgeøya are in flood plains or valley bottoms that are seasonally free of any ice. Pressurized groundwater stems from high hydraulic potential because the water originates in upland areas. This is why pingos typically form in lowlands surrounded by topographic relief (French, 2007).

Studies on Svalbard's pingos (Liestøl, 1977; Burr et al, 2009) hypothesize that they form via injection of ice from groundwater accumulating beneath glaciers' terminal moraines and flowing towards the coast. This is made possible by unfrozen pockets within the permafrost, particularly in regions where the sediment is salty and thus capable of remaining unfrozen at 0°C. It can thus be inferred that pingo icings and glacial icings in the same region have the same source of groundwater, and that they would share similar characteristics. Such a relation can be seen in the pingos of Adventdalen and Foxfonna glacier, a glacier whose terminal moraine is in Adventdalen (Burr et al, 2009).

Methane amounts are likely impacted by glacial hydrology on Spitsbergen. Further sampling on glacial icings should be undertaken. However, in this analysis, only one glacial icing had confirmed methane in winter of 2019. Therefore, pingo icings and pingos will be focused on as confirmed sources of methane ventilation. The glacial spring measured in Foxfonna had gaseous methane at 3.1%. The pingos located further down the valley of this glacier have very high levels of methane. Similarly, the glacial icings of Tungebreen and Tavlebreen had no methane at all. These icings are located above the valley of Grøndalen (figure 5.6), which only had one pingo icing where methane was detected.

Although pingos are limited by elevation and by topography, geology may also influence their formation. Based on the geographical distribution, pingos have formed in geology of varying origins. They only occur in tertiary, Triassic, Jurassic, Cretaceous, Devonian, Neoproterozoic, and Mesoproterozoic lithology on Svalbard. Pingos are not found in calcareous Carboniferous or Permian rocks. This is because the rate of water discharge is so high that it is impossible for icings to form (Hjelle, 1993). Nordenskiöld Land is chiefly composed of tertiary bedrock, with sandstone and shale rock types and many coal deposits. Shale is impermeable but porous, and sandstone is highly permeable, which facilitates the transport of groundwater. This would expedite the formation of pingos. It can therefore be implied that the hydrology and structure of pingos are influenced by lithology. Conversely, it is also possible that pingos can form in other stratigraphic regions, but have simply been limited because of Svalbard's mountainous terrain and the fact that it is 60% covered by glaciers and ice caps (figure 2.2). Andrée Land in particular has so many fault lines that it is possible that their presence will facilitate the formation of pingos in the future.

A GIS spatial distribution was created for pingos and fault lines on Svalbard (figure 5.9). This is because other studies (Burr et al, 2009; Yoshikawa and Harada, 1995; Yoshikawa et al, 1996) have found pingos in Asia that develop along minor faults. The formation of Asian pingos may be comparable to the ones in Svalbard. In the GIS spatial analysis, 33.7% of all pingos on Spitsbergen were located within 1 kilometer of the nearest fault line. Many of these pingos such as the ones in Andrée Land (figure 5.11) occurred parallel to the fault lines in or alongside the valleys. Weakness in bedrock allows for more efficient travel of groundwater, which would facilitate the growth of pingos. This theory cannot be hypothesized for the island of Edgeøya due to the lack of data on fault lines east of the Svalbard archipelago. In the future, more pingos should be visited in the field, particularly the far north of Spitsbergen in Andrée Land as well the south-central coast of Wedel Jarlsberg Land. More data should be collected on minor fault lines on Svalbard to consider if their presence facilitates or prevents the flow of groundwater.

Only one pingo icing was found in Andrée Land, which is notable because Andrée Land only has normal (and assumed normal) fault lines. In Nordenskiöld Land and Wedel Jarlsberg Land, many pingo icings were found. These regions also had reverse fault lines. Predominantly, pingo icings occur near reverse fault lines. There may be a link between pingos and

compressional tectonics that are responsible for reverse faulting and easier transport of geothermal heat and groundwater. Extensional tectonics resulting in normal faulting and transverse faults were only associated with one pingo icing. This might mean that the most active pingos systems at present are associated with particular tectonic settings. Reasons for this are unclear. Furthermore, data on fault lines in Svalbard is not complete, particularly underneath glaciers and in inaccessible regions such as the north of Spitsbergen.

The hypothesis that pingos will form closer to the sides of the basin while upper valley pingos tend to form closer to the center of the valley was tested. In several valleys such as Reindalen, Adventdalen, and Vogtdalen, the distribution of pingos followed this physical arrangement (figure 5.14). This is not true in all cases, and the distribution of pingos along the width of the valleys had a bimodal distribution (figure 5.15). It is possible that marine sediments within the Holocene marine limit causes pingos to preferentially develop near the sides. Research should be conducted on pock marks in fjords to consider their distributions.

On Svalbard, pingos are only located on the islands of Edgeøya and Spitsbergen. Two-thirds of these pingos are located in Nordenskiöld Land. Furthermore, although there is a significant concentration of pingos on the northern coast of Spitsbergen and on Edgeøya, no observable icings exist near them. This may suggest that the pingos are inactive, like the ones found in upper Reindalen on Nordenskiöld Land that have begun to collapse. Groundwater icings were only found near fourteen pingos across Svalbard. These icings were only found on Spitsbergen, not Edgeøya. Furthermore, only four pingos with associated icings were not on the peninsula of Nordenskiöld Land. Because these icings appear even in late winter, mean annual air temperature and precipitation are likely not relevant to their formation. Nordenskiöld Land is also host to several major fault lines, such as the Billefjorden Fault Zone. Measuring the full effects of fault zones on near-surface hydrogeology remain very challenging (Bense et al, 2013).

Fault zones are capable of being hydraulic conduits connecting shallow and deep geological environments, as well as creating barriers to prevent flow. These features presumably would affect the formation of pingos. In Svalbard, excess groundwater near pingos is generally found near reverse faults, possibly indicating that compressional tectonics facilitate groundwater movement. Furthermore, it does not appear that pingos are found at the valley margins in lower valleys and closer to the center in upper valleys due to thick marine infill in the Holocene marine

limit. Based on the observed distribution (figure 5.14), there does not appear to be a specific reason thus far for widthwise formation of pingos across valleys. There are likely multiple factors influencing whether pingos form along the margins of valleys or near the center of valleys. Such factors may include regional lithology, porosity or weakness of bedrock, presence of terminal glacier moraines, or other variations in valley topography.

## 6.2 Compounds Associated with Methane

The principal components analysis showed that four major components justify the relationships between compounds and elements associated to methane (section 5.4). This factor analysis was conducted using winter data and not summer data because more methane is released in the winter (October to May) than in the summer (June to September). This is because the influx of water from summer melt dilutes the fluids (Hodson et al, 2019). It is estimated that methane ventilates in winter at a rate 2.5 times higher than in summer (Shakhov et al, 2010).

Furthermore, field sites were more difficult to access during the melt season and so more sampling was completed in March to May of 2019 when there was still snow and ice on the ground. In the first component, it is evident that methane and carbon dioxide were closely correlated (table 5.1). This is an expected outcome because both compounds are products of microbiological activity. Other artifacts of component 1 include high chloride loading and a negative sulfate loading. The former suggests the presence of marine pore waters. This is expected from the sediment infill in the lower valley, as it was submerged during the Last Glacial Maximum. The latter suggests sulfate removal processes such as sulfate reduction since this occurs at redox conditions similar to those conducive to methanogenesis (Purdy et al, 2003). Therefore, factor 1 appears to show a strong link between methanogenesis, the presence of marine pore water, and other low redox processes within marine sediments.

The second component shows that total dissolved solids are dominated by sodium and bicarbonate. It can be assumed that sodium is present due to marine sediments, but the sodium to chloride ratios exceed those of standard ocean water. Sodium concentrations are significantly higher than chloride due to the release of sodium by weathering. In central Spitsbergen, sodium ions not supplied by marine pore waters are released by albite weathering, which is driven by sulfide oxidation (Yde et al, 2008). Sulfide oxidation produces iron oxy-hydroxides, and these were frequently observed in upper Adventdalen. Furthermore, the cation composition is not

dominated by magnesium, calcium, or potassium. The likely explanation is that they have replaced sodium via ion exchange processes.

Apart from component 1, only component 3 indicates an association with methane. The strongest loading of this component is from ammonium, suggesting perhaps a link with the diagenesis of organic matter in the sediments. As organic matter matures, N is released in its reduced form as  $\text{NH}_4^+$  in clay environments. High ammonium concentration has been found to be associated with hydrocarbons in sandstone environments in the United States (Williams et al, 1992) and thus this may be applicable to Svalbard as well. Component 4 had a strong loading from manganese. Manganese is a primary electron acceptor for organic matter oxidation in anaerobic sedimentary environments. The reduction of manganese is correlated with the growth of methanogenic bacteria (Myers and Nealson, 1988). Methane-producing archaeobacteria have been coupled with manganese, iron, nitrate, and sulfate reduction in submarine permafrost on the Siberian shelf (Winkel et al, 2018). It is therefore possible that manganese may be important for the growth of methanogenic bacteria in Svalbard.

Methane has a positive linear correlation with deuterium and excess carbon dioxide. These can both be considered key predictive variables. Originally  $\delta^{18}\text{O}$  was run with carbon dioxide and not deuterium, because  $\delta^{18}\text{O}$  is generally associated with methanogenesis (Jahren et al, 2004).  $\delta^{18}\text{O}$  is a function of the water in which it forms, and thus is an excellent indicator of historical water temperatures. The production of methane by archaeobacteria, or methanogenesis, is a process involving isotopic fractionation (Kietäväinen and Purkamo, 2015). However, the multiple regression test showed that deuterium predicted the variance of methane much better than  $\delta^{18}\text{O}$  did. 91.0% of the variance in methane can be predicted with deuterium and carbon dioxide in a multiple regression model while it was only 87% when  $\delta^{18}\text{O}$  was run. Carbon dioxide is integral because its association with methane means that microbiological activity is relevant. Deuterium is a key variable because it is an abundant isotope in ocean water and can be used to trace the geographical source of water (Goncharuk, 2013). Deuterium is negative compared to the VSMOW standard, indicating it is depleted in comparison to seawater and therefore behaves differently than standard seawater. Pingos in the lower part of Adventdalen are located within the Holocene marine limit, and have salty sediments that are enriched with deuterium.

The benefits of being able to use deuterium and carbon dioxide to predict methane removes the costly process of analyzing water samples using a mass spectrometer. It also removes the time-consuming process of converting gaseous methane into aqueous methane. Aqueous methane cannot be measured directly because it would destroy the delicate membrane of a traditional detector.

### 6.3 Limitations

The limitations of this study include mechanical failure, lack of summer data, one site being previously drilled, and lack of fault data east of Svalbard. Compounds and stable isotopes for the Adventdalen sites from the years 2018 and 2019 would have been valuable for the statistical analysis completed for this paper, but this data cannot be represented due to mechanical error. Furthermore, the factor analysis and linear regression were only done for the winter seasons of 2015-2017. Although less methane is released in the summer due to microbial activity, there is less data from fewer days because it is logistically very difficult to reach the sites in the summer months. Of the data collected in winter 2019, it is possible that the site of Trodalen was compromised. In Trodalen, 4.1% gaseous methane was measured. However, this site had been drilled the previous day and the water within had equilibrated. It is therefore possible that the actual methane amount was originally higher. For this reason, multiple methane measurements were not taken in drilled sites because the water equilibrated shortly after becoming exposed. Springs that are naturally exposed can have multiple measurements, but the sites visited in 2019 were kept pressurized when sealed and so further measurements would not have been accurate. Multiple measurements at these sites would have been informative, but it was not possible to perform them.

Finally, the lack of fault data east of Svalbard meant that the island of Edgeøya could not be included in the theory that pingos preferentially develop near major fault lines. The predictive model is built within the marine limit, and therefore may not be effective when analyzing data outside of the marine limit. This is due to a lack of deuterium in sediments that were not submerged during the Last Glacial Maximum. However, at present there is not enough data collected on pingos outside of the marine limit in Svalbard. This model likely would not work on glacial icings on Svalbard because of a similar lack of data.

## 7. Conclusion

Permafrost underlies 90%-100% of Svalbard's land area. Furthermore, an estimated 60% of the archipelago is covered by glaciers. Permafrost worldwide contains approximately 1672 gigatons of carbon, which is roughly equivalent to the total contained within plants and the atmosphere (Mackelprang et al, 2011). When permafrost thaws, carbon is released into the atmosphere. Although most of this is released in the form of carbon dioxide, significant amounts are released as methane, which has a greenhouse warming effect 28 times higher than that of carbon dioxide (Mau et al, 2017). Methane hydrates are stored at low temperatures and at high pressures on the ocean floor as well as in sub-permafrost reservoirs on land in polar regions. Methane is also created by reduction from anaerobic microorganisms in permafrost environments. In the High Arctic Norwegian archipelago of Svalbard, permafrost features known as pingos contain up to 59% gaseous methane (figure 5.7). On land that has been isostatically uplifted, it is believed that pingos form from once-submerged pockmarks that ventilate methane. Pingos are not common features in permafrost environments, as they require specific conditions in order to form and to maintain their unusual structures. It is estimated that there are 11 000 in the world.

Pingos in Svalbard were analyzed using a combination of observations made in the field, water sampling, statistical analysis, and GIS analysis. An exhaustive list was created for each pingo in Svalbard and factors identified such as distance to nearest fault line, elevation, and presence of groundwater icings. In the field, pingos in Nordenskiöld Land were visited and their late-winter groundwater icings sampled. The varying amounts of methane were mapped to consider the spatial distribution of methane in Nordenskiöld Land. Much research in Svalbard has been completed on this peninsula due to ease of access, but there is little information on pingos or icings across the rest of Svalbard. Ninety-eight pingos were identified on the islands of Edgeøya and Spitsbergen on Svalbard. The pingos on the central peninsula of Nordenskiöld Land on Spitsbergen have been studied the most. Many of these pingos ventilate large amounts of methane, but not all. Little is understood about the formation of these pingos or what factors influence their hydrology. Several studies have posited that pingos form alongside (or near) major fault zones (Mackay, 1987; Yoshikawa et al, 2003), a fact that is corroborated by 33.7% of all pingos on Spitsbergen being found within one kilometer of a major fault line.

Predicting where methane can be found and its amount released would be vital in understanding methane reservoirs across the rest of Spitsbergen. A predictive model was created for methane ventilation from pingos in Adventdalen within the Holocene marine limit. The equation  $y_{CH_4} = 195.1 + 0.019x_{CO_2} + 1.758x_D$  likely cannot be used for pingos located higher up valleys, as there would be little to no deuterium present in these sediments. In the future, more pingos should be visited in the field, particularly sites that are not part of Nordenskiöld Land. Notable sites would be the far north of Spitsbergen in Andrée Land as well the south-central coast of Wedel Jarlsberg Land. Both of these regions have pingos with associated groundwater icings that should be measured for methane. Furthermore, more data should be collected on minor fault lines on Svalbard to consider if their presence facilitates or prevents the flow of groundwater. Finally, research should be conducted on pockmarks in the fjords of Svalbard, to be compared and contrasted with ventilation on-land.

Despite the limitations, satisfactory data was collected for the purpose of this research paper. The intentions of this thesis were to understand and quantify the amount of methane released from pingos in Svalbard in the year 2019. By creating a database of pingos in Svalbard and analyzing the factors affecting them, perhaps more can be understood about the field of Arctic hydrology. With changing climate patterns, it is important to understand and predict the behaviour of methane in the Arctic. Svalbard has several sources of methane ventilation such as pingos. The IPCC has declared Svalbard a region that is climatically very sensitive due to risk factors such as less albedo from less cover of snow and sea ice as well as polar amplification (Aas et al, 2016). If a better understanding of the source and behaviour of methane ventilation is developed, it could provide insights on what the consequences of a warming climate would be for Svalbard and other regions in the High Arctic. Developing information on how pingos form and what factors lead to higher rates of methane ventilation could assist in mitigating the effects of greenhouse gases in a sensitive region of the world.

## 8. References

- Aagaard, K., Foldvik, A., and Hillman, S.R. "The West Spitsbergen Current: disposition and water mass transformation." *Journal of Geophysical Research: Oceans* 92.C4 (1987): 3778-3784.
- Aas, Kjetil Schanke, Dunse, T., Collier, E., Schuler, T., Berntsen, T.K., Kohler, J. and Luks, B. "The climatic mass balance of Svalbard glaciers: a 10-year simulation with a coupled atmosphere-glacier mass balance model." *The Cryosphere* 10.3 (2016): 1089-1104.
- Anthony, Katey M. Walter, Anthony, P., Grosse, G., and Chanton, J. "Geologic methane seeps along boundaries of Arctic permafrost thaw and melting glaciers." *Nature Geoscience* 5, no. 6 (2012): 419.
- Benn, D, and Evans, D. *Glaciers and Glaciation*. Routledge (2014).
- Bense, V. F., Gleeson, T., Loveless, S. E., Bour, O. and Scibek, J. "Fault zone hydrogeology." *Earth-Science Reviews* 127 (2013): 171-192.
- Berndt, C., Feseker, T., Treude, T., Krastel, S., Liebetrau, V., Niemann, H., Bertics, V.J., Dumke, I., Dünnbier, K., Ferré, B. and Graves, C. "Temporal constraints on hydrate-controlled methane seepage off Svalbard." *Science* 343, no. 6168 (2014): 284-287.
- Bøggild, C., Lüthje, M., and Holmes, J. "Albedo observations with large concentrations of Black Carbon in high Arctic snow packs from Svalbard." *63rd Eastern Snow Conference, Newark, Delaware, USA* (2007).
- Bondevik, Stein, Mangerud, J., Ronnert, L. and Salvigsen, O. "Postglacial sea-level history of Edgeøya and Barentsøya, eastern Svalbard." *Polar Research* 14.2 (1995): 153-180.
- Brown, J., Ferrians, O. J., Heginbottom, J. A., and Melnikov, E. S. Circum-Arctic Map of Permafrost and Ground Ice Conditions. Circum-Pacific Map Series, CP-45, scale 1: 10,000,000. United States Geological Survey (1997).
- Burr, Devon M., Tanaka, K.L., and Yoshikawa, Kenji. "Pingos on Earth and Mars." *Planetary and Space Science* 57.5-6 (2009): 541-555.

Christiansen, Hanne H., Humlum, Ole, and Eckerstorfer, Markus. "Central Svalbard 2000–2011 meteorological dynamics and periglacial landscape response." *Arctic, Antarctic, and Alpine Research* 45.1 (2013): 6-18.

Crémière, A, Lepland, A., Chand, S., Sahy, D., Condon, D.J., Noble, S.R., Martma, T., Thorsnes, T., Sauer, S. and Brunstad, H. "Timescales of methane seepage on the Norwegian margin following collapse of the Scandinavian Ice Sheet." *Nature Communications* 7 (2016): 11509.

Eckerstorfer, Markus, and Christiansen, Hanne H. "The “High Arctic maritime snow climate” in central Svalbard." *Arctic, Antarctic, and Alpine Research* 43, no. 1 (2011): 11-21.

Elverhøi, Anders, Andersen, E.S., Dokken, T., Hebbeln, D., Spielhagen, R., Svendsen, J.I., Sørflaten, M., Rørnes, A., Hald, M. and Forsberg, C.F. "The growth and decay of the Late Weichselian ice sheet in western Svalbard and adjacent areas based on provenance studies of marine sediments." *Quaternary Research* 44.3 (1995): 303-316.

Forwick, Matthias, Baeten, Nicole J., and Vorren, Tore O. "Pockmarks in Spitsbergen fjords." *Norwegian Journal of Geology/Norsk Geologisk Forening* 89 (2009).

Frederick, J. M., and Buffett, B. A. "Taliks in relict submarine permafrost and methane hydrate deposits: Pathways for gas escape under present and future conditions." *Journal of Geophysical Research: Earth Surface* 119.2 (2014): 106-122.

French, Hugh M. *The periglacial environment*. John Wiley & Sons (2007).

Goncharuk, Vladyslav V., Kavitskaya, A.A., Romanyukina, I.Y. and Loboda, O.A. "Revealing water’s secrets: deuterium depleted water." *Chemistry Central Journal* 7.1 (2013): 103.

Haldorsen, Sylvi, Heim, M., Dale, B., Landvik, J.Y., van der Ploeg, M., Leijnse, A., Salvigsen, O., Hagen, J.O. and Banks, D. "Sensitivity to long-term climate change of subpermafrost groundwater systems in Svalbard." *Quaternary research* 73.2 (2010): 393-402.

Hambrey, Michael J., Murray, T., Glasser, N.F., Hubbard, A., Hubbard, B., Stuart, G., Hansen, S. and Kohler, J. "Structure and changing dynamics of a polythermal valley glacier on a

centennial timescale: Midre Lovénbreen, Svalbard." *Journal of Geophysical Research: Earth Surface* 110.F1 (2005).

Hansen, Brage Bremset, Isaksen, K., Benestad, R.E., Kohler, J., Pedersen, Å.Ø., Loe, L.E., Coulson, S.J., Larsen, J.O. and Varpe, Ø. "Warmer and wetter winters: characteristics and implications of an extreme weather event in the High Arctic." *Environmental Research Letters* 9 (2014).

Hodson, Andrew J., and Ferguson, Robert I. "Fluvial suspended sediment transport from cold and warm-based glaciers in Svalbard." *Earth Surface Processes and Landforms* 24.11 (1999): 957-974.

Hodson, Andrew J., Nowak, A., Holmlund, E., Redeker, K., Turchyn, A.V., and Christiansen, H.H. "Seasonal dynamics of Methane and Carbon Dioxide evasion from an open system pingo: Lagoon Pingo, Svalbard." *Frontiers in Earth Science* (2019).

Hodson, Andrew J., Nowak, A., Senger, K., Redeker, K., Christiansen, H.H., Jessen, S., Hornum, M., Betlem, P., Thornton, S., Turchyn, A.V., Olaussen, S., and Marca, A. "Direct escape of sub-permafrost methane through open system pingos and its contribution to atmospheric emissions." *Frontiers in Earth Science* (in review).

Hong, Wei-Li, Torres, M. E., Carroll, J., Crémière, A., Panieri, G., Yao, H., and Serov, P. "Seepage from an arctic shallow marine gas hydrate reservoir is insensitive to momentary ocean warming." *Nature communications* 8 (2017): 15745.

Hjelle, Audun. *Geology of Svalbard*. Norwegian Polar Institute (1993).

Ingólfsson, Ó. "Fingerprints of Quaternary glaciations on Svalbard." *Geological Society, London, Special Publications* 354.1 (2011): 15-31.

Jahren, A. H., LePage, B.A., and Werts, S.P. "Methanogenesis in Eocene Arctic soils inferred from  $\delta^{13}\text{C}$  of tree fossil carbonates." *Palaeogeography, Palaeoclimatology, Palaeoecology* 214, no. 4 (2004): 347-358.

Kietäväinen, Riikka, and Purkamo, Lotta. "The origin, source, and cycling of methane in deep crystalline rock biosphere." *Frontiers in microbiology* 6 (2015): 725.

Liestøl, Olav. "Pingos, springs, and permafrost in Spitsbergen." *Norsk Polarinstitutt Arbok* 1975 (1977): 7-29.

Liestøl, Olav. "Open-system pingos in Spitsbergen." *Norsk Geografisk Tidsskrift-Norwegian Journal of Geography* 50.1 (1996): 81-84.

Ling, Feng, Wu, Q., Zhang, T. and Niu, F. "Modelling open-talik formation and permafrost lateral thaw under a thermokarst lake, Beiluhe Basin, Qinghai-Tibet Plateau." *Permafrost and Periglacial Processes* 23.4 (2012): 312-321.

Lønne, Ida, and Lyså, Astrid. "Deglaciation dynamics following the Little Ice Age on Svalbard: Implications for shaping of landscapes at high latitudes." *Geomorphology* 72.1-4 (2005): 300-319.

Mackay, J. Ross. "Some mechanical aspects of pingo growth and failure, western Arctic coast, Canada." *Canadian Journal of Earth Sciences* 24.6 (1987): 1108-1119.

Mackelprang, Rachel, Waldrop, M.P., DeAngelis, K.M., David, M.M., Chavarria, K.L., Blazewicz, S.J., Rubin, E.M., and Jansson, J.K. "Metagenomic analysis of a permafrost microbial community reveals a rapid response to thaw." *Nature* 480, no. 7377 (2011): 368.

Marín-Moreno, H., Minshull, T. A., Westbrook, G. K., Sinha, B., & Sarkar, S. "The response of methane hydrate beneath the seabed offshore Svalbard to ocean warming during the next three centuries." *Geophysical Research Letters* 40.19 (2013): 5159-5163.

Matsuoka, Norikazu, Sawaguchi, Shin-ichi, and Yoshikawa, Kenji. "Present-day periglacial environments in central Spitsbergen, Svalbard." *Geographical Review of Japan* 77.5 (2004): 276-300.

Mau, S., Römer, M., Torres, M.E., Bussmann, I., Pape, T., Damm, E., Geprägs, P., Wintersteller, P., Hsu, C.W., Loher, M. and Bohrmann, G. "Widespread methane seepage along the continental margin off Svalbard-from Bjørnøya to Kongsfjorden." *Scientific reports* 7 (2017): 42997.

Metfies, Katja, von Appen, W. J., Kiliyas, E., Nicolaus, A., & Nöthig, E. M. "Biogeography and photosynthetic biomass of arctic marine pico-eukaryotes during summer of the record sea ice minimum 2012." *PLoS One* 11.2 (2016): e0148512.

Moholdt, Geir, Nuth, C., Hagen, J.O. and Kohler, J. "Recent elevation changes of Svalbard glaciers derived from ICESat laser altimetry." *Remote Sensing of Environment* 114.11 (2010): 2756-2767.

Müller, Oliver, Bang-Andreasen, T, White, R.A. III, Elberling, B., Taş, N., Kneafsey, T., Jansson, J.K., and Øvreås, L. "Disentangling the complexity of permafrost soil by using high resolution profiling of microbial community composition, key functions and respiration rates." *Environmental microbiology* 20, no. 12 (2018): 4328-4342.

Myers, Charles R., and Nealson, Kenneth H. "Bacterial manganese reduction and growth with manganese oxide as the sole electron acceptor." *Science* 240.4857 (1988): 1319-1321.

Nordli, Ø., Przybylak, R., Ogilvie, A. E., and Isaksen, K. "Long-term temperature trends and variability on Spitsbergen: the extended Svalbard Airport temperature series, 1898–2012." *Polar Research* 33.1 (2014): 21349.

Norwegian Polar Institute. "Topographic Map of Svalbard." 2015.

Osterkamp, T. "The recent warming of permafrost in Alaska." *Global and Planetary Change* 49.3-4 (2005): 187-202.

Pälli, Anja, Moore, J. C., Jania, J., Kolondra, L., and Glowacki, P. "The drainage pattern of Hansbreen and Werenskioldbreen, two polythermal glaciers in Svalbard." *Polar Research* 22.2 (2003): 355-371.

Paull, Charles K., Ussler, W., Dallimore, S.R., Blasco, S.M., Lorenson, T.D., Melling, H., Medioli, B.E., Nixon, F.M. and McLaughlin, F.A. "Origin of pingo-like features on the Beaufort Sea shelf and their possible relationship to decomposing methane gas hydrates." *Geophysical Research Letters* 34.1 (2007).

Piepenburg, Dieter. "Recent research on Arctic benthos: common notions need to be revised." *Polar Biology* 28, no. 10 (2005): 733-755.

Portnov, Alexey, Vadakkepuliymbatta, S., Mienert, J., and Hubbard, A. "Ice-sheet-driven methane storage and release in the Arctic." *Nature communications* 7 (2016): 10314.

Portnov, Alexey, Smith, A.J., Mienert, J., Cherkashov, G., Rekant, P., Semenov, P., Serov, P. and Vanshtein, B. "Offshore permafrost decay and massive seabed methane escape in water depths > 20 m at the South Kara Sea shelf." *Geophysical Research Letters* 40.15 (2013): 3962-3967.

Portnov, Alexey, Mienert, Jurgen, and Serov, Pavel. "Modeling the evolution of climate-sensitive Arctic subsea permafrost in regions of extensive gas expulsion at the West Yamal shelf." *Journal of geophysical research: Biogeosciences* 119.11 (2014): 2082-2094.

Purdy, K. J., Nedwell, D.B., and Embley, T.M. "Analysis of the sulfate-reducing bacterial and methanogenic archaeal populations in contrasting Antarctic sediments." *Appl. Environ. Microbiol.* 69.6 (2003): 3181-3191.

Riedel, Michael, Wallmann, K., Berndt, C., Pape, T., Freudenthal, T., Bergenthal, M., Bünz, S. and Bohrmann, G. "In situ temperature measurements at the Svalbard Continental Margin: Implications for gas hydrate dynamics." *Geochemistry, Geophysics, Geosystems* 19.4 (2018): 1165-1177.

Rønning, Olaf I. *The flora of Svalbard*. Norsk polarinstitutt (1996).

Røthe, Torgeir O., Bakke, J., Støren, E. W., and Bradley, R. S. "Reconstructing Holocene glacier and climate fluctuations from lake sediments in Vårfluesjøen, northern Spitsbergen." *Frontiers in Earth Science* 6 (2018).

Røthe, Torgeir O., Bakke, J., Vasskog, K., Gjerde, M., D'Andrea, W.J. and Bradley, R.S. "Arctic Holocene glacier fluctuations reconstructed from lake sediments at Mitrahallvøya, Spitsbergen." *Quaternary Science Reviews* 109 (2015): 111-125.

Serov, Pavel, Portnov, A., Mienert, J., Semenov, P., and Ilatovskaya, P. "Methane release from pingo-like features across the South Kara Sea shelf, an area of thawing offshore permafrost." *Journal of Geophysical Research: Earth Surface* 120.8 (2015): 1515-1529.

Shakhova, Natalia Evgenievna, Semiletov, I.P., Salyuk, A.N., Bel'cheva, N.N. and Kosmach, D.A. "Methane anomalies in the near-water atmospheric layer above the shelf of East Siberian Arctic shelf." *Doklady Earth Sciences*. Vol. 415. No. 1. MAIK Nauka/Interperiodica, 2007.

Shakhova, Natalia Evgenievna, Semiletov, I., Salyuk, A., Yusupov, V., Kosmach, D. and Gustafsson, Ö. "Extensive methane venting to the atmosphere from sediments of the East Siberian Arctic Shelf." *Science* 327.5970 (2010): 1246-1250.

Stotler, Randy L., Frapre, S.K., Ahonen, L., Clark, I., Greene, S., Hobbs, M., Johnson, E., Lemieux, J.M., Peltier, R., Pratt, L. and Ruskeeniemi, T. "Origin and stability of a permafrost methane hydrate occurrence in the Canadian Shield." *Earth and Planetary Science Letters* 296.3-4 (2010): 384-394.

van Everdingen, Robert O. "Multi-Language Glossary of Permafrost and Related Ground Ice Terms." Calgary: University of Calgary (1998).

van Pelt, Ward, JJ, Pohjola, V.A., and Reijmer, C.H. "The changing impact of snow conditions and refreezing on the mass balance of an idealized Svalbard glacier." *Frontiers in Earth Science* 4 (2016): 102.

Voiland, Adam. "Arctic Amplification." *Earth Observatory*, NASA (2013).  
[earthobservatory.nasa.gov/images/81214/arctic-amplification](http://earthobservatory.nasa.gov/images/81214/arctic-amplification).

Wadham, J. L., Hodson, A.J., Tranter, M. and Dowdeswell, J.A. "The hydrochemistry of meltwaters draining a polythermal-based, high Arctic glacier, south Svalbard: I. The ablation season." *Hydrological Processes* 12.12 (1998): 1825-1849.

Wagner, Dirk, and Liebner, S. "Methanogenesis in Arctic permafrost habitats." *Handbook of hydrocarbon and lipid microbiology* (2010): 655-663.

Wallmann, Klaus, Riedel, M., Hong, W.L., Patton, H., Hubbard, A., Pape, T., Hsu, C.W., Schmidt, C., Johnson, J.E., Torres, M.E. and Andreassen, K. "Gas hydrate dissociation off Svalbard induced by isostatic rebound rather than global warming." *Nature communications* 9.1 (2018): 83.

Westbrook, G.K., Thatcher, K.E., Rohling, E.J., Piotrowski, A.M., Pälike, H., Osborne, A.H., Nisbet, E.G., Minshull, T.A., Lanoisellé, M., James, R.H. and Hühnerbach, V., D. Green, R.E. Fisher, A.J. Crocker, A. Chabert, C. Bolton, A. Beszczynska-Möller, C. Berndt, A. Aquilina. "Escape of methane gas from the seabed along the West Spitsbergen continental margin." *Geophysical Research Letters* 36.15 (2009).

Winkel, Matthias, Mitscherling, J., Overduin, P.P., Horn, F., Winterfeld, M., Rijkers, R., Grigoriev, M.N., Knoblauch, C., Mangelsdorf, K., Wagner, D. and Liebner, S. "Anaerobic methanotrophic communities thrive in deep submarine permafrost." *Scientific reports* 8.1 (2018): 1291.

Williams, L.B., Wilcoxon, B.R., Ferrell, R.E. and Sassen, R. "Diagenesis of ammonium during hydrocarbon maturation and migration, Wilcox Group, Louisiana, USA." *Applied Geochemistry* 7.2 (1992): 123-134.

Woo, Ming-ko. *Permafrost Hydrology*. Springer Science & Business Media (2012).

Yde, J.C., Riger-Kusk, M., Christiansen, H.H., Knudsen, N.T. and Humlum, O. "Hydrochemical characteristics of bulk meltwater from an entire ablation season, Longyearbreen, Svalbard." *Journal of Glaciology* 54.185 (2008): 259-272.

Yoshikawa, Kenji. "Notes on open-system pingo ice, Adventdalen, Spitsbergen." *Permafrost and Periglacial Processes* 4.4 (1993): 327-334.

Yoshikawa, Kenji, and Harada, Koichiro. "Observations on nearshore pingo growth, Adventdalen, Spitsbergen." *Permafrost and Periglacial Processes* 6.4 (1995): 361-372.

Yoshikawa, Kenji, White, D., Hinzman, L., Goering, D., Petrone, K., Bolton, W., Ishikawa, N. and Plummer, N.L. "Water in permafrost; case study of aufeis and pingo hydrology in discontinuous permafrost." *Proceedings of the International Conference on Permafrost. Zurich, Switzerland* (2003).

Zimov, S. A., Schuur, E. A.G., and Chapin, F. S. "Climate Change: Permafrost and the Global Carbon Budget." *Science* 312.5780 (2006): 1612-1613.

## 9. Appendix

Table 0.1. The locations and parameters measured at icings in Nordenskiöld Land.

Site Name	Longitude (N)	Latitude (E)	Elevation (m)	CO <sub>2</sub> (mg/L)	PH
Lagoon East	78°14'22.0" N	15°45'17.3" E	4	74	7.8
Lagoon West	78°14'27.1" N	15°45'06.6" E	2	106	7.8
DGPN	78°15'28.9" N	16°23'47.4" E	200	231	4.5
Innerhytta	78°11'21.1" N	16°20'38.5" E	75	241	7.1
GDP-1	77°59'44.3" N	14°40'24.2" E	45	1	8.9
GDP-2	77°59'47.7" N	14°40'15.3" E	42	0	7.3
Tungebreen	77°57'56.1" N	14°56'35.8" E	162	0	7.8
Tavlebreen	77°59'04.8" N	15°10'16.5" E	167	9	8.4
Trodalen	78°04'12.2" N	15°14'25.5" E	47	11	9
BLT-1 North	78°10'37.1" N	16°00'02.3" E	24	30	6.9
BLT-2 South	78°10'05.9" N	15°59'20.3" E	44	33	7
BLT-3 South	78°10'03.0" N	15°59'13.4" E	54	36	7
Fox-2	78°09'51.0" N	16°06'06.3" E	91	11	7.4
RP-E	78°11'37.7" N	16°28'19.6" E	94	234	5.1
RP-W	78°11'39.7" N	16°26'16.9" E	77	236	6
NP-1	78°03'11.4" N	16°33'34.9" E	161	NM	6.3
NP-2	78°03'07.7" N	16°33'18.8" E	161	NM	8
Fox-1	78°09'38.5" N	16°06'16.5" E	221	0	7.9
Reindalen-P	78°03'16.2" N	16°33'22.2" E	161	NM	7.8
Kalvdalen-1	77°55'32.5" N	15°11'51.5" E	91	191	4.17
Kalvdalen-2	77°55'32.3" N	15°11'51.5" E	87	176	3.59
Rypefjellbreen	77°53'50.9" N	15°18'10.8" E	34	4	7.93
Lake 1	77°53'47.5" N	15°34'24.2" E	1	10	7.12
Lake 2	77°53'53.8" N	15°36'53.5" E	1	16	5.46
Lake 3	77°54'31.4" N	15°35'16.7" E	1	32	5.88
Røystoppdalen	77°57'24.0" N	16°07'21.4" E	96	57	5.89

Table 0.1 continued.

<b>Site Name</b>	<b>Longitude (N)</b>	<b>Latitude (E)</b>	<b>Conductivity (mS/cm)</b>	<b>O2 (mg/L)</b>	<b>OP (MV)</b>	<b>CH4 (%)</b>
Lagoon East	78°14'22.0" N	15°45'17.3" E	8	0.56	-360	30.51
Lagoon West	78°14'27.1" N	15°45'06.6" E	9	0.62	-183	59.04
DGPN	78°15'28.9" N	16°23'47.4" E	22.4	0.84	1.45	0.105
Innerhytta	78°11'21.1" N	16°20'38.5" E	9.31	0.84	-91	15.21
GDP-1	77°59'44.3" N	14°40'24.2" E	1.993	0	-283	2.20
GDP-2	77°59'47.7" N	14°40'15.3" E	2.44	1.12	-110	0
Tungebreen	77°57'56.1" N	14°56'35.8" E	0.243	15.6	60.3	0
Tavlebreen	77°59'04.8" N	15°10'16.5" E	0.055	5.05	60.3	0
Trodalen	78°04'12.2" N	15°14'25.5" E	1.604	3.61	-61	4.10
BLT-1 North	78°10'37.1" N	16°00'02.3" E	2.146	15	152.8	0
BLT-2 South	78°10'05.9" N	15°59'20.3" E	3.2	16.4	173	0
BLT-3 South	78°10'03.0" N	15°59'13.4" E	1.202	8.7	171	0
Fox-2	78°09'51.0" N	16°06'06.3" E	0.81	13.04	167.5	0
RP-E	78°11'37.7" N	16°28'19.6" E	23.7	1.3	122.3	0.50
RP-W	78°11'39.7" N	16°26'16.9" E	21.7	0.18	-51.8	7.10
NP-1	78°03'11.4" N	16°33'34.9" E	0.857	1.33	73.3	0
NP-2	78°03'07.7" N	16°33'18.8" E	0.013	7.31	56.2	0
Fox-1	78°09'38.5" N	16°06'16.5" E	611	0	-110	3.10
Reindalen-P	78°03'16.2" N	16°33'22.2" E	0.82	3.44	82.9	NM
Kalvdalen-1	77°55'32.5" N	15°11'51.5" E	73	2	160	0
Kalvdalen-2	77°55'32.3" N	15°11'51.5" E	5.98	0.32	260	0
Rypefjellbreen	77°53'50.9" N	15°18'10.8" E	3.64	0.35	-397	2.70
Lake 1	77°53'47.5" N	15°34'24.2" E	1.66	9.31	163	0.20
Lake 2	77°53'53.8" N	15°36'53.5" E	1.76	16.21	140	0.10
Lake 3	77°54'31.4" N	15°35'16.7" E	1.97	19.54	231	0.10
Røystoppdalen	77°57'24.0" N	16°07'21.4" E	1.49	1.2	-270	4.80

Table 0.2. Data taken from River Pingo, Innerhytta Pingos, Førstehytta Pingo, and Lagoon Pingo from years 2015 to 2017 (Hodson et al, in review).

Sample ID	d13C-CH4	pH	O2	ORP	CH4	CO2	dO-H2O	dH-H2O	NH4
RP 21/04/17	-54.43	NM	1.11	133.8	4.78	126.08	-15.4	-110.8	1.61
RP 15/04/17	-55.02	7.32	BD	-64.1	6.12	119.93	-14.9	-108.6	1.87
RP 17/03/17	BD	8.15	BD	-25.1	0.61	97.17	-15.1	-109.2	0.82
RP 19/03/17	BD	7.22	2.18	113.1	0.97	98.88	-15.3	-108.5	0.65
RP 16/4/16	-55.57	7.21	0.31	-191.8	32.36	313.87	-13.84	-99.5	2.76
RP 12/4/16	-51.53	7.06	0.17	-12.1	24.86	420.20	-14.0	-100.8	2.07
RP 12/4/15	-55.89	7.61	0.68	-74.9	20.15	161.97	-13.9	-99.8	1.86
IH 23/09/17	-53.81	NM	BD	BD	16.91	797.56	-13.47	-97.49	BD
IH 19/04/17	-55.9	7.16	0.77	-35.4	25.02	352.18	-13.7	-99.2	2.37
IH 15/04/17	-56.1	7.11	BD	-118.5	BD	BD	-13.6	-98.9	2.47
IH 17/03/17	-55.65	6.81	0.3	-67.4	27.64	309.46	-13.6	-99.4	2.47
IH 21/4/16	-57.79	6.89	0.43	-189	29.85	799.09	-13.97	-100.4	2.22
IH 12/4/16	-51.75	7.07	0.23	-20.7	41.26	560.96	-13.5	-97.6	2.51
IH 22/4/15	-49.72	6.88	0.22	-20.7	42.73	870.09	-13.3	-95.2	2.33
FHP 3/10/17	-64.16	7.1	0.1	-38.1	11.85	641.26	-14.45	-103.78	0.90
FHP 13/9/17	-64.74	NM	BD	BD	16.51	770.35	-14.41	-103.4	0.71
FHP 5/9/17	-58.54	9.81	0.21	-135.9	13.26	582.67	-14.3	-101.7	0.62
FHP 19/4/17	-48.17	7.35	1.11	-195.2	15.32	294.17	-14.4	-106.5	1.06
FHP 15/4/17	-52.3	7.34	BD	-180.3	15.14	251.76	-15.0	-106.0	1.37
FHP 16/3/17	-54.02	7.35	0.34	-140.1	14.02	207.64	-14.8	-105.3	0.76
FHP 21/4/16	-67.38	7.31	0.49	-238	18.08	368.41	-14.58	-104.3	1.18
FHP 12/4/16	-55.27	7.2	0.3	-199	14.10	448.18	-14.7	-104.6	1.14
FHP 9/4/16	-56.11	7.21	0.31	-191.8	16.61	416.95	-14.7	-104.5	0.97
FHP 10/5/15	-67.12	7.81	0.9	-202	13.35	464.11	-15.7	-111.2	1.12
FHP 23/4/14	BD	7.25	0.6	-212.2	35.67	733.02	-14.4	-101.6	BD
LP 21/10/17	BD	7.69	BD	-53.6	7.26	209.88	-14.71	-103.16	1.61
LP 28/9/17	-70.67	NM	0.13	-34.6	5.99	110.33	-14.49	-101.53	2.43
LP 24/8/17	-69.79	7.7	0.13	-242.7	6.13	174.78	-14.35	-101.75	1.77
LP 6/8/17	BD	7.69	0.2	-312.9	5.41	147.14	-14.91	-105.08	1.41
LP 19/4/17	-55.61	7.07	2.44	-229.1	9.5	73.39	-15.1	-107.5	2.38
LP 15/4/17	-48.31	8.05	BD	-202.2	6.3	62.49	-15.2	-108.0	2.28
LP 16/3/17	-61.95	7.71	1.71	-180.9	9.631	74.29	-15.5	-107.7	2.23
LP 10/4/16	-66.81	7.94	0.48	-206.7	14.48	162.38	-15.2	-106.4	2.62

Table 0.2 continued.

Sample ID	Si	HCO3	Cl-	PO4	SO4	Na	K	Mg	Ca
RP 21/04/17	3.08	228.8	1563.301	BD	2878.1	1016.9	7.89	517.7	459.3
RP 15/04/17	3.03	280.6	1523.9	BD	1947.1	916.2	6.89	352.8	380.7
RP 17/03/17	2.91	305.4	775.1	BD	3665.8	562.5	6.30	537.4	533.9
RP 19/03/17	2.85	235.7	779.9	BD	3509.2	538.8	5.96	494.6	480.2
RP 16/4/16	2.75	2699.1	1542.7	0.044	40.1	1910.8	4.99	13.8	31.6
RP 12/4/16	2.74	2766.1	1509.1	0.030	43.2	1976.9	4.95	13.0	30.7
RP 12/4/15	2.02	3711.1	1449.0	0.043	24.3	2268.5	6.92	20.1	32.6
IH 23/09/17	BD	3416.8	1549.2	0.00	4.7	2233.7	10.2	15.4	26.0
IH 19/04/17	2.86	1996.7	1529.3	0.00	0.0	1693.1	4.14	12.72	19.27
IH 15/04/17	2.84	2022.6	1493.7	0.00	0.0	1682.5	4.13	11.73	18.41
IH 17/03/17	2.88	2042.9	1515.5	0.00	1.4	1703.0	4.48	12.32	18.92
IH 21/4/16	2.85	3930.7	1382.6	0.08	38.6	2307.4	3.70	20.63	39.99
IH 12/4/16	2.80	3989.2	1406.9	0.01	14.5	2334.6	3.54	20.19	39.61
IH 22/4/15	BD	3874.8	1485.7	0.02	17.4	2360.9	5.30	17.74	28.12
FHP 3/10/17	3.45	3615.2	1083.2	BD	9.9	2013.9	10.4	13.4	20.3
FHP 13/9/17	2.98	3586.7	1064.7	BD	9.1	1994.3	9.9	13.2	19.9
FHP 5/9/17	3.54	3401.0	985.4	BD	8.5	1870.8	5.3	14.4	20.4
FHP 19/4/17	3.92	2430.2	1104.8	BD	11.3	1584.5	5.89	13.36	20.43
FHP 15/4/17	4	2393.5	1126.0	BD	12.1	1580.3	7.41	15.16	20.13
FHP 16/3/17	3.72	2363.3	1066.6	BD	15.6	1535.9	5.43	13.68	21.05
FHP 21/4/16	3.82	4178.1	1058.1	0.027	48.5	2192.4	5.54	21.57	40.65
FHP 12/4/16	3.90	4129.0	1099.2	0.053	63.7	2206.4	5.76	21.52	41.97
FHP 9/4/16	3.86	3870.4	1095.7	0.070	59.3	2105.8	5.69	21.60	40.88
FHP 10/5/15	2.49	4542.4	1071.3	0.082	36.1	2336.1	10.59	23.81	30.81
FHP 23/4/14	BD	7562.5	1025.8	BD	31.7	3429.9	11.999	25.75	39.58
LP 21/10/17	2.69	3671.1	241.1	2.2731	92.0	1503.7	26.96	25.23	11.63
LP 28/9/17	2.69	3720.0	524.0	2.8187	99.4	1694.9	35.38	29.43	11.16
LP 24/8/17	2.61	3766.2	674.1	2.5521	119.2	1806.0	28.1	38.4	12.8
LP 6/8/17	2.90	3910.0	175.2	1.7534	101.2	1568.0	18.9	22.8	10.2
LP 19/4/17	3.94	3541.3	391.6	2.914	120.7	1559.0	25.4	28.1	12.9
LP 15/4/17	4.16	3482.1	417.8	3.443	128.2	1554.1	26.3	29.3	13.3
LP 16/3/17	3.97	2341.0	395.9	2.544	114.5	1127.9	19.7	21.0	9.2
LP 10/4/16	4.21	5251.2	541.2	1.488	247.7	2256.6	39.2	63.2	38.2

Table 0.2 continued.

Sample ID	Sr	Fe	Mn	TDS	pCO2	SI calcite	SI gypsum	SI Fe(OH)3	SI siderite
RP 21/04/17	5956.2	880.3	5155.5	6799.5	-1.99	-0.08	-0.03	-1.42	-0.62
RP 15/04/17	5450.5	786.8	3836.7	5456.2	-2.03	0.13	-0.19	-1.02	-0.4
RP 17/03/17	6429.9	449.0	6231.9	6516.9	-2.85	1.03	0.12	1.14	0.11
RP 19/03/17	6386.9	577.0	6540.6	6148.4	-2.01	-0.02	0.08	-1.49	-0.75
RP 16/4/16	2745.4	914.5	77.6	7269.8	-0.90	0.03	-2.77	-1.63	0.23
RP 12/4/16	1837.7	718.1	67.4	7454.5	-0.74	-0.12	-2.76	-2.18	-0.02
RP 12/4/15	1181.7	732.1	582.9	8948.7	-1.17	0.53	-3.04	-0.66	0.53
IH 23/09/17	3005.6	535.8	38.1	8606.6	-0.59	-0.41	-4.06	-2.56	-0.18
IH 19/04/17	3012.3	476.3	6.4	6071.3	-0.98	-0.5	BD	-1.96	-0.13
IH 15/04/17	3192.2	492.3	5.4	6059.4	-0.92	-0.58	BD	-2.1	-0.16
IH 17/03/17	2977.7	499.5	8.0	6132.6	-0.62	-0.86	-4.58	-2.99	-0.45
IH 21/4/16	3282.2	443.1	5.9	9239.6	-0.43	-0.35	-3.04	-3.01	-0.36
IH 12/4/16	3054.1	408.3	6.5	9337.6	-0.6	-0.18	-3.48	-2.52	-0.21
IH 22/4/15	1930.3	581.2	4.4	9295.7	-0.42	-0.43	-3.45	-2.92	-0.25
FHP 3/10/17	3709.9	186.0	15.4	8162.0	-0.67	-0.16	-3.59	-2.73	-0.53
FHP 13/9/17	3281.8	971.6	16.3	8090.4	-0.72	-0.12	-3.63	-1.87	0.24
FHP 5/9/17	4229.3	14.38	BD	7614.6	-0.92	0.06	-3.63	BD	BD
FHP 19/4/17	4231.7	1008.9	63.1	6125.9	-1.08	-0.03	-3.45	-1.13	0.41
FHP 15/4/17	4013.7	998.9	71.6	6093.6	-1.08	-0.05	-3.42	-1.16	0.39
FHP 16/3/17	3934.3	988.4	82.8	5949.7	-1.09	-0.02	-3.29	-1.13	0.4
FHP 21/4/16	4377.3	651.4	41.9	9135.8	-0.82	0.38	-2.65	-1.62	0.22
FHP 12/4/16	4236.6	576.3	72.7	9148.6	-0.71	0.28	-2.51	-1.99	0.07
FHP 9/4/16	4572.6	425.5	67.8	8681.5	-0.75	0.26	-2.54	-2.07	-0.06
FHP 10/5/15	2446.3	739.2	127.8	8060.3	-1.29	0.77	-2.93	-0.15	0.73
FHP 23/4/14	BD	333.8	11.4	12130.8	BD	BD	BD	BD	BD
LP 21/10/17	1188.8	333	34.9	6950.8	-1.24	0.2	-2.82	-0.76	0.28
LP 28/9/17	1144.3	252	23.6	7518.1	-1.24	0.18	-2.84	-0.89	0.15
LP 24/8/17	1456.1	25	16.0	7870.9	-1.24	0.23	-2.72	-1.9	-0.85
LP 6/8/17	1291.4	24	0.5	7291.6	-1.22	0.17	-2.85	-1.93	-0.86
LP 19/4/17	1639.8	145	32.5	7025.9	-0.64	-0.38	-2.66	-2.93	-0.66
LP 15/4/17	1493.0	65	51.8	6978.0	-1.63	0.58	-2.64	-0.45	-0.15
LP 16/3/17	992.0	101	25.8	4940.3	-1.45	-0.01	-2.73	-1.07	-0.26
LP 10/4/16	1312.5	205	120.9	10394.2	-1.36	1.02	-2.04	-0.39	0.28

Table 0.3. A list of the 98 pingos found on Spitsbergen and Edgeøya.

<b>Region</b>	<b>Valley</b>	<b>Elevation (m)</b>	<b>Location from Center</b>	<b>Distance from Ocean (km)</b>	<b>Distance from Nearest Fault Line (km)</b>
Nordenskiöld Land	Reindalen	39	0.01	3.2	19.8
Nordenskiöld Land	Reindalen	40	0.11	2.73	19.4
Nordenskiöld Land	Reindalen	61	0.06	2.96	19
Nordenskiöld Land	Reindalen	13	0.13	0.97	18.7
Nordenskiöld Land	Reindalen	8	0.19	0.36	18.9
Nordenskiöld Land	Reindalen	122	0.53	26.4	11.05
Nordenskiöld Land	Reindalen	161	0.18	34.4	5.89
Nordenskiöld Land	Reindalen	138	0.46	35.1	4.94
Nordenskiöld Land	Reindalen	136	0.52	35.2	4.8
Nordenskiöld Land	Reindalen	133	0.64	35.5	4.57
Nordenskiöld Land	Reindalen	153	0.87	37.7	2.86
Nordenskiöld Land	Reindalen	136	0.81	39.4	1.14
Nordenskiöld Land	Reindalen	163	0.28	40.2	0.35
Nordenskiöld Land	Reindalen	156	0.57	41.7	0.86
Nordenskiöld Land	Reindalen	168	0.52	41.8	0.92
Nordenskiöld Land	Reindalen	182	0.64	41.9	0.96
Nordenskiöld Land	Reindalen	180	0.65	45.3	4.87
Nordenskiöld Land	Reindalen	100	0.04	18	20.4
Nordenskiöld Land	Vassdalen	73	0.72	2.65	13.1
Nordenskiöld Land	Grøndalen	43	0.63	7.75	10.3
Nordenskiöld Land	Grøndalen	44	0.65	8.88	11
Nordenskiöld Land	Grøndalen	56	0.72	9.01	11.1
Nordenskiöld Land	Grøndalen	59	0.65	9.22	11.3
Nordenskiöld Land	Grøndalen	60	0.27	9.57	11.9
Nordenskiöld Land	Grøndalen	71	0.18	9.89	12.4
Nordenskiöld Land	Hollendardalen	66	0.52	5.74	10.5
Nordenskiöld Land	Adventdalen	2	0.2	0.05	10.6
Nordenskiöld Land	Adventdalen	4	0.2	0.05	10.7
Nordenskiöld Land	Adventdalen	23	0.27	2.51	11.2
Nordenskiöld Land	Adventdalen	31	0.11	5.28	8.62
Nordenskiöld Land	Adventdalen	81	0.65	14.3	0.48
Nordenskiöld Land	Adventdalen	162	0.66	24.4	1.01
Nordenskiöld Land	Adventdalen	77	0.91	19.3	0.79

Table 0.3 continued.

<b>Region</b>	<b>Valley</b>	<b>Elevation (m)</b>	<b>Location from Center</b>	<b>Distance from Ocean (km)</b>	<b>Distance from Nearest Fault Line (km)</b>
Nordenskiöld Land	Eskerdalen	83	0.6	12.4	3.78
Nordenskiöld Land	Eskerdalen	94	0.32	12.4	3.58
Nordenskiöld Land	Eskerdalen	101	0.26	12.4	3.41
Nordenskiöld Land	Eskerdalen	109	0.19	12.4	3.1
Nordenskiöld Land	Eskerdalen	79	0.47	15.2	3.32
Nordenskiöld Land	Eskerdalen	89	0.56	15.2	2.82
Nordenskiöld Land	Trehøgddalen	102	0.95	15.8	3.84
Nordenskiöld Land	Brentskaret	139	0.87	26.1	0.45
Nordenskiöld Land	Brentskaret	149	0.27	24.7	1.05
Nordenskiöld Land	De Geerdalen	198	0.86	10.6	0.48
Nordenskiöld Land	De Geerdalen	213	0.85	11	0.66
Nordenskiöld Land	Vendomdalen	70	0.76	21.9	13.4
Nordenskiöld Land	Vendomdalen	76	0.45	21	10.6
Nordenskiöld Land	Fulmardalen	107	0.95	31.1	7.96
Nordenskiöld Land	Agardhdalen	21	0.91	6.14	0.21
Nordenskiöld Land	Kjellströmdalen	10	0.83	13.7	11.4
Nordenskiöld Land	Kjellströmdalen	39	0.5	18.8	14.8
Nordenskiöld Land	Kjellströmdalen	29	0.6	18.8	15
Nordenskiöld Land	Kjellströmdalen	59	0.4	20.2	14.2
Nordenskiöld Land	Kjellströmdalen	68	0.19	20.6	13.6
Nordenskiöld Land	Lundströmdalen	97	0.57	14.9	7.08
Nordenskiöld Land	Lundströmdalen	35	0.78	11.8	7.98
Nordenskiöld Land	Skutdalen	122	0.91	17.2	11.8
Nordenskiöld Land	Aurdalen	40	0.97	7.16	3.65
Nordenskiöld Land	Aurdalen	42	0.77	7.06	3.67
Nordenskiöld Land	Aurdalen	38	0.61	7.05	3.65
Nordenskiöld Land	Berzeliusdalen	23	0.85	4.12	3.56
Oscar II Land	Kaffiøyra	38	0.71	3.25	0.15
Haakon VII Land	Watnelieøyra	3	0.3	0.48	0.28
Haakon VII Land	Watnelieøyra	12	0.89	5	0.88
Haakon VII Land	Kronprinshallet	39	0.68	0.94	1.02
Haakon VII Land	Kronprinshallet	45	0.62	1.04	0.88

Table 0.3 continued.

<b>Region</b>	<b>Valley</b>	<b>Elevation (m)</b>	<b>Location from Center</b>	<b>Distance from Ocean (km)</b>	<b>Distance from Nearest Fault Line (km)</b>
Wedel Jarlsberg Land	Chamberlindalen	20	0.86	2.41	1.3
Wedel Jarlsberg Land	Chamberlindalen	15	0.79	3	1.1
Wedel Jarlsberg Land	Chamberlindalen	18	0.9	3.9	0.67
Wedel Jarlsberg Land	Dunderdalen	45	0.24	9.05	1.55
Wedel Jarlsberg Land	Dunderdalen	37	0.21	11.2	0.77
Andrée Land	Vogtdalen	1	0.65	3.14	1.95
Andrée Land	Vogtdalen	10	0.41	4.21	2.02
Andrée Land	Vogtdalen	34	0.98	6.62	1.78
Andrée Land	Vogtdalen	46	0.97	7.27	1.95
Andrée Land	Vatnedalen	79	0.96	6.11	0.76
Andrée Land	Forkdalen	49	0.44	2.5	0.17
Andrée Land	Forkdalen	62	0.31	2.37	0.09
Andrée Land	Møydalen	137	0.52	6.65	0.47
Andrée Land	Purpurdalen	35	0.64	1.8	0.69
Andrée Land	Woodfjorddalen	7	0.83	3.72	4.53
Andrée Land	Woodfjorddalen	1	0.74	4.14	4.9
Andrée Land	Woodfjorddalen	18	0.13	5.15	5.48
Andrée Land	Woodfjorddalen	10	0.45	14.4	7.85
Andrée Land	Piræusdalen	110	0.23	10.6	7.6
Andrée Land	Stjørdalen	120	0.49	7.23	1.07
Andrée Land	Stjørdalen	129	0.34	7.33	1.03
Andrée Land	Stjørdalen	159	0.26	7.33	0.74
Andrée Land	Stjørdalen	163	0.42	9.25	0.88
Andrée Land	Stjørdalen	159	0.5	9.25	1.11
Andrée Land	Junkerdalen	106	0.67	7.3	3.7
Andrée Land	Verdalen	43	0.23	1.46	3.21
Olav V Land	Ebbadalen	30	0.79	4	7.4
Edgeøya	Raddedalen	59	0.93	11.3	76.5
Edgeøya	Smelledalen	45	0.71	10.1	80.2
Edgeøya	Smelledalen	43	0.85	11.2	83.4
Edgeøya	Raundalen	58	0.84	11.1	90.1
Edgeøya	Atndalen	106	0.42	10.9	80.1
Edgeøya	Tydalen	109	0.92	12	86.3